Deformation Pattern of the Northern Sector of the Malta Escarpment (Offshore SE Sicily, Italy): Fault Dimension, Slip Prediction, and Seismotectonic Implications

Salvatore Gambino, Giovanni Barreca, Felix Gross, Carmelo Monaco, Sebastian Krastel, Marc-André Gutscher

HAL Id: hal-03451160
https://hal.univ-brest.fr/hal-03451160v1

Submitted on 29 Nov 2021

Check for
updates

Deformation Pattern of the Northern Sector of the Malta Escarpment (Offshore SE Sicily, Italy): Fault Dimension, Slip Prediction, and Seismotectonic Implications

Salvatore Gambino[1], Giovanni Barreca[1,2]*, Felix Gross[3,4], Carmelo Monaco[1,2,5], Sebastian Krastel[3] and Marc-André Gutscher[6]

[1]Department of Biological, Geological and Environment Sciences, University of Catania, Catania, Italy, [2]CRUST—Interuniversity Center for 3D Seismotectonics with Territorial Applications, Chieti, Italy, [3]Institute of Geosciences, Kiel University, Kiel, Germany, [4]Center for Ocean and Society, Kiel University, Germany, Kiel, [5]Istituto Nazionale di Geofisica e Vulcanologia, Osservatorio Etneo, Catania, Italy, [6]Laboratoire Géosciences Ocean, UMR6538 CNRS/University of Brest, Plouzané, France

Marine seismic reflection data coupled with on-land structural measurements improve our knowledge about the active deformation pattern of the northern sector of the Malta Escarpment, a bathymetric and structural discontinuity in the near-offshore of Eastern Sicily. As favourably oriented to be reactivated within the Neogene Africa–Europe convergence, it is believed that the Malta Escarpment has a significant role in the recent seismotectonic framework of the Western Ionian Basin and the Hyblean foreland domain of SE Sicily, where some of the largest and most destructive Mediterranean earthquakes are located according to available historical catalogs. Offshore seismic data along with bathymetric grids illuminate the shallow subseafloor setting and allow more accurate mapping of the seafloor expression of previously identified faults in the area. The seismic interpretation and the near-fault sediment pattern analysis provide constraints on fault 3D geometries as well as on their through-time tectonic activity, suggesting also that part of the observed deformation may have been caused by nontectonic processes. Identified faults form currently an E-dipping, roughly N–S trending, and 60 km-long extensional belt deforming the seafloor with a significant displacement amount in the Ionian offshore between Catania and Siracusa. 3-dimensional parameters of faults were then used to derive expected magnitudes and their reactivation propensity. Empirical scaling relationships and forward methods point to a high seismic potential for the detected fault as well as predict the fault slip behavior according to the field-derived differential stress. This combined analysis along with faults displacement measurements pointed out how the longest and most continuous fault could be capable of generating M > 7 seismic events, putting forward strong seismotectonic implications for the adjacent and densely populated Hyblean Plateau. The expected magnitude and the estimated recurrence time interval are compatible with those inferred for large historical earthquakes in the area even if other offshore seismic sources cannot be ruled out.

Keywords: seismic potential, fault slip prediction, 3D data modeling, recent/active tectonics, field deformation pattern, offshore seismic investigation, malta escarpment

INTRODUCTION

The Malta Escarpment in the Western Ionian Basin (Southern Italy, **Figure 1**) is a 300 km long structural and bathymetric discontinuity inherited from the Permian–Triassic paleotectonic setting (Scandone et al., 1981; Fabbri et al., 1982; Casero et al., 1984) separating at that time two sectors of the African plate with different crustal thickness/rheology: the thinned/oceanic Ionian Basin to the east and the Hyblean continental "promontory" to the west. More recently, this inherited discontinuity has been partly reactivated in the frame of the Nubia–Eurasia convergence

dynamics and forms an impressive NNW–SSE trending submarine fault-scarp in the near-offshore of the densely populated SE Sicily. Although debated, several studies have considered this tectonic structure as a potential source for major historical earthquakes and tsunamis in Eastern Sicily in historical times (Piatanesi and Tinti, 1998; Bianca et al., 1999; Azzaro and Barbano, 2000; Argnani and Bonazzi, 2005; Argnani et al., 2012). For this reason, it is considered a key feature for the seismotectonics of SE Sicily and the Western Ionian Basin. Based on macroseismic data and numerical modeling (Mulargia et al., 1985; Barbano and Rigano, 2001; Sirovich and Pettenati, 2001; DISS working group,
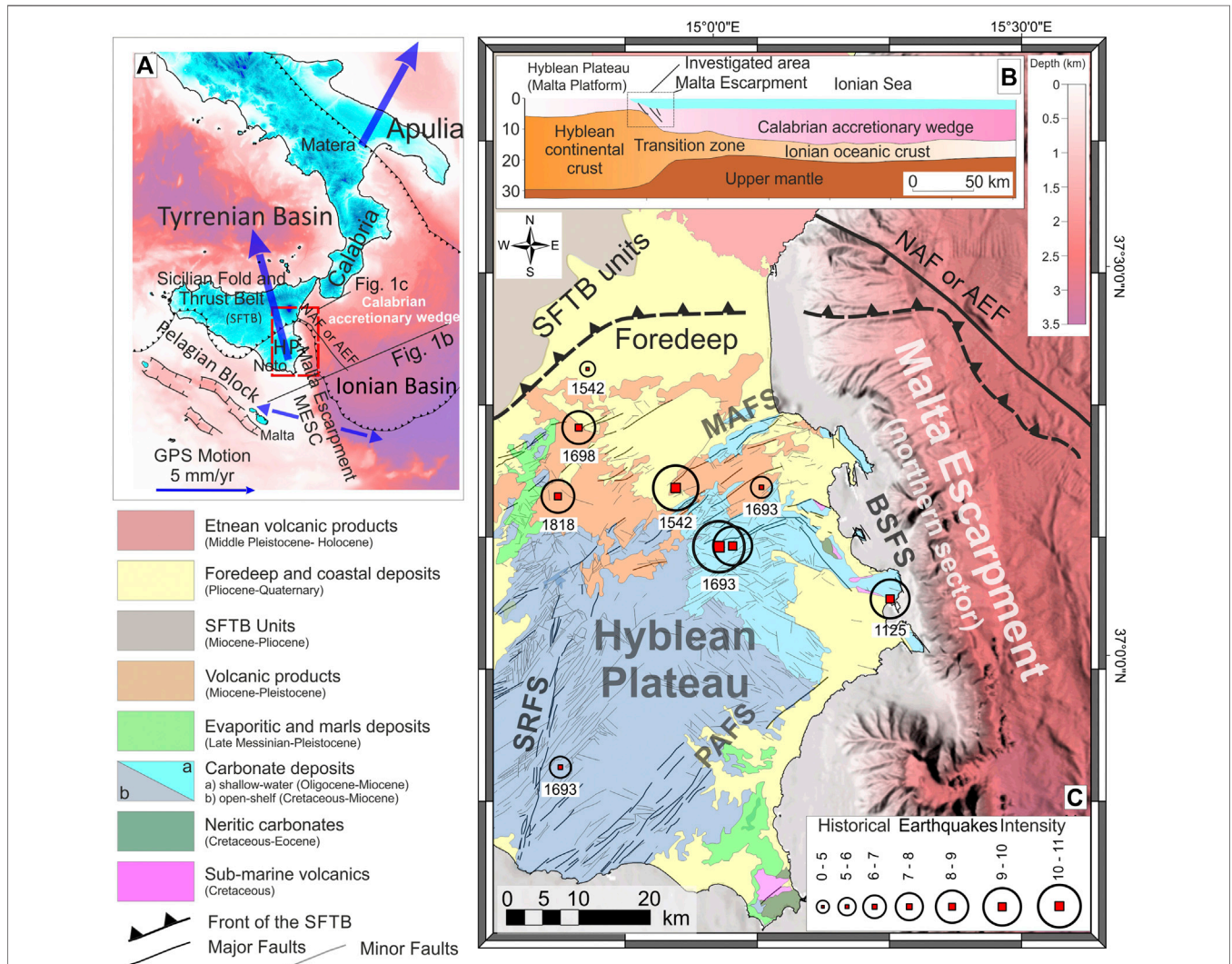
FIGURE 1 | (A) The Malta Escarpment framed in the structural setting of the central Mediterranean region. Large blue arrows indicate diverging geodetic velocities (see Ward 1994; Mastrolembo et al., 2014; D'Agostino and Selvaggi, 2004; Grenerczy et al., 2005; Palano et al., 2012) measured in the lower plate (Hyblean Plateau and Apulia Block) of the collisional system. The diverging motion resolves a resultant WNW–ESE extension along the E-Sicily/Western Ionian Basin domain (small blue arrows) where the inherited NNW–SSE trending Malta Escarpment occurs. **(B)** Structurally, the investigated area places at the shallow portion of an ancient (Permo–Triassic) ocean–continent transition domain where the Malta Escarpment is widely considered to be a Mesozoic passive margin related either to E-W spreading of an Ionian oceanic ridge (see Catalano et al., 2001), or as has been recently suggested a transform margin, related to NE-SW extension (Gallais et al., 2011; Dellong et al., 2018). **(C)** Structural setting of the Malta Escarpment footwall block, the SE Sicily. Black circles indicate the epicentres of the most energetic historical earthquakes occurred in the area. Acronyms are as follows: SRFS, Scicli–Ragusa Faults System; PAFS, Pozzallo–Avola Faults System; MAFS, Monterosso–Agnone Faults System; BSFS, Brucoli–Siracusa Faults Systems; NAF of AEF, North Alfeo Fault or Alfeo Etna Fault (Gutscher et al., 2016; Polonia et al., 2016).

2018) and according to CPTI15 reference catalog (Rovida et al., 2016), epicentres of most historical events (e.g., February 4, 1169, and January 11, 1693, events, among the most destructive) have been positioned in the footwall of this tectonic feature. Whatever the source, Southeastern Sicily, forming the footwall block of the Malta Escarpment, is one of the most seismically active areas in Europe having experienced many destructive earthquakes (M > 5.5) and associated tsunamis (Boschi et al., 1995; Tinti et al., 2001; Tinti et al., 2004; Jenny et al., 2006).

Despite the many authors mentioned above, identifying the Malta Escarpment as the most likely fault system as having produced most of the historical and recent earthquakes, evidence of recent/active tectonics has so far remained elusive. This is due to the absence or scant evidence of faulted Quaternary sediments on-land and to the unavailability of offshore data capable of adequately imaging the shallow subseafloor environment, where the youngest sediments occur. Accordingly, the seismic potential of the Malta Escarpment along with its structural architecture, fault dimension, and kinematics, as well as deformation rate, remains poorly understood. In this study, we present a detailed investigation of the structural architecture of the northernmost sector of the Malta Escarpment by using marine geophysical data with unprecedented resolution, field constraints, and data modeling. Interpretation of 2D seismic reflection profiles provides further constraints on the tectonic setting of the investigated area allowing for the classification of the activity and the geometric parameters of the detected faults. All available 2D seismic data were analyzed to build-up a consistent 2½D model of the fault planes. Reconstructed fault surfaces combined with stress orientations coming from field investigations performed alongshore Southeastern Sicily allow us to evaluate their seismic potential by assessing the likelihood of their reactivation.

GEOLOGICAL SETTING

The Malta Escarpment (hereinafter MESC) is a steep, E-facing submarine slope with a total bathymetric drop of more than 3,000 m (**Figure 1A**). Structurally, it marks the ocean–continent transition zone as its separates two sectors of the African margin with different lithospheric thicknesses: the thinned (oceanic) Ionian Basin to the east and the Hyblean continental promontory to the west (Dellong et al., 2018, **Figure 1B**). This transition zone is a remnant of a paleotectonic setting related to the Permo–Triassic opening of the Neo-Tethys (Şengör, 1979) and to the subsequent Jurassic–Cretaceous spreading stage (Ben-Avraham and Grasso, 1991; Catalano et al., 2001; Gallais et al., 2011; Dellong et al., 2018). Successively, this passive paleomargin has been reactivated during the Neogene convergence between Africa and Eurasia plates as it is oriented transversally (NNW–SSE) to the roughly E–W trending of the advancing front of the resulting collisional system (**Figure 1A**). The progressive foreland-ward migration of the collisional system involved the ocean–continent preorogenic configuration leading to the shaping of the Sicilian fold and thrust belt (SFTB in **Figure 1A**) to the west and the Calabrian accretionary wedge to the east

(**Figure 1A**). In this context, the impingement of the collisional front against the MESC paleotopography probably allowed the passive margin to be reactivated by oblique extension during the Plio–Quaternary (Scandone et al., 1981; Fabbri et al., 1982; Casero et al., 1984; Bianca et al., 1999; Palano et al., 2012). The footwall block of the MESC is locally known as the Hyblean Plateau (**Figure 1C**), and it represents the emergent of a larger foreland domain, the Pelagian Block (Burollet et al., 1978; Ben-Avraham and Grasso, 1991, **Figure 1A**), a 25–30 km thick continental crustal compartment of the African margin. The Hyblean Plateau sedimentary covers consist of 10 km-thick, Meso–Cenozoic open-shelf to shallow-water carbonate sequences, hosting several intercalations of volcanic products (Patacca et al., 1979; Bianchi et al., 1987; Grasso et al., 2004). The Quaternary top sequences are widespread all over the plateau edges on the coastal domains where they are generally preserved within fault-bounded structural depressions (Grasso and Lentini, 1982, **Figure 1C**).

Structurally, the Hyblean Plateau consists of a rigid, highly fractured crustal intender delimited by the front of the Sicilian Fold and Thrust Belt to the north–west and by the MESC to the east (**Figure 1C**). This structural pattern, strongly influenced by inherited Mesozoic structures (Grasso and Reuther, 1988; Henriquet et al., 2019) is dominated by major structural features and associated minor structures pervasively deforming the plateau. The NW and SE margins are controlled by large, NE–SW trending normal fault systems (Monterosso–Agnone and Pozzallo–Avola fault systems, respectively, see Cultrera et al., 2015, **Figure 1C**) which have been associated with flexural bulging processes (Pedley and Grasso, 1992; Cogan et al., 1989; Billi et al., 2006). To the west, the Hyblean Plateau is sliced by a roughly N–S-oriented strike-slip fault belt known as the Scicli–Ragusa fault system (Ghisetti and Vezzani, 1980; Grasso and Reuther, 1988). The eastern margin is structurally controlled by an NNW–SSE, E-dipping extensional fault system (Brucoli–Siracusa fault system, **Figure 1C**) encompassing the MESC and its associated on-land structures. Here, Plio–Quaternary tectonic activity is testified by the occurrence of syntectonic sediments within extensional basins mainly occurring on the footwall of MESC, whereas in the hanging wall, located offshore, Quaternary deformation was imaged through deep-penetrating but low-resolution seismic lines (Bianca et al., 1999; Adam et al., 2000; Argnani and Bonazzi, 2002; Argnani and Bonazzi, 2005). More recently, some authors framed the MESC in the Ionian subduction dynamics, interpreting it as the upper crustal expression of a deep-seated lateral tear in the Ionian lithosphere (Subduction Transform Edge Propagator—STEP fault, see Argnani and Bonazzi, 2005; Govers and Wortel, 2005; Polonia et al., 2012; Argnani et al., 2013). However, since STEP fault propagation typically produces alongside vertical-axis structural rotations (see Govers and Wortel, 2005; Barreca et al., 2016), the adjacent paleomagnetically unrotated Hyblean Plateau (Grasso et al., 1983; Cifelli et al., 2004) doesn't support a STEP behavior for the MESC. Late Quaternary sense of motion along the MESC is also still debated primarily due to the impossibility of measuring African plate movements in the offshore and also due to the lack of clear temporal and kinematic constraints on-land. Based on
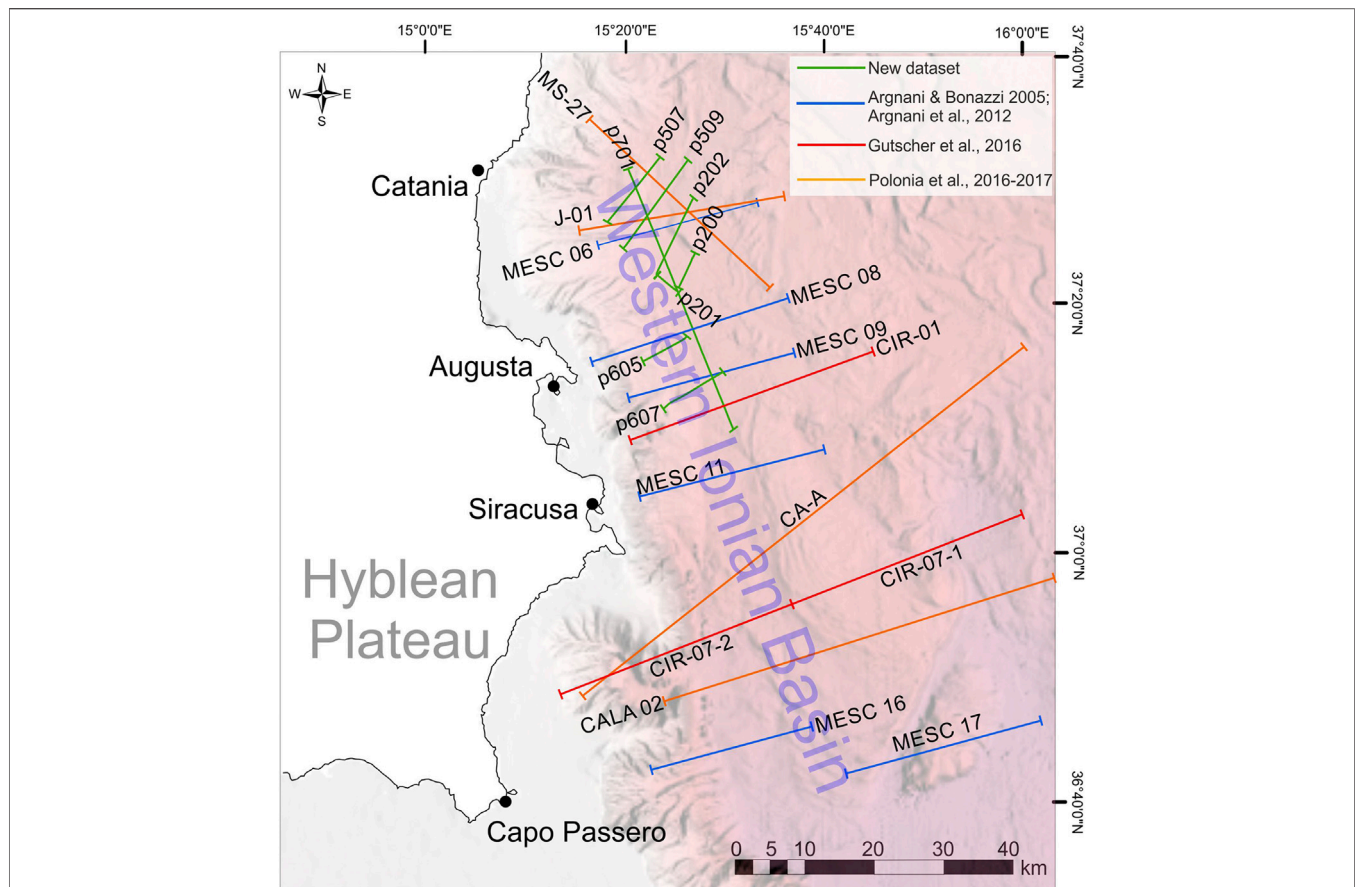
FIGURE 2 | Location of the interpreted seismic dataset in the offshore of SE Sicily. The dataset includes new seismic profiles (green lines) and previously published geophysical data.

neotectonic observations, Adam et al. (2000) suggested that on-shore structures related to the MESC fault system are characterized by left-lateral kinematics. Although doubtful, this assertion appears to be consistent with seismological data (Amato et al., 1995; Musumeci et al., 2014). On the contrary, regional-scale geodynamic interpretations (e.g., Doglioni et al., 2001) and seismological (Presti et al., 2013) and geodetic data (Palano et al., 2012) suggest a right-lateral component of motion for the considered fault system. Diverging GPS vectors measured on the lower plate (including the Hyblean and Adria blocks, see Ward 1994; Mastrolembo et al., 2014; D'Agostino and Selvaggi, 2004; Grenerczy et al., 2005) indicates the latter as a crustal domain extending according to the resultant ESE–WNW-oriented vector (**Figure 1A**). In this geodynamic frame, the NNW–SSE trending MESC should have been reactivated with an oblique (right-lateral transtensional) component of deformation.

DATA AND METHODS

The analyzed data primarily consist of seismic reflection lines recorded during various marine geophysical cruises performed in the Western Ionian Basin (**Figure 2**). Interpreted seismic data

consist of high-resolution seismic profiles sounded in the frame of the CIRCEE-HR project (R/V le Suroît, October 2013, see also Gutscher et al., 2016) and Poseidon expedition POS496 (R/V Meteor, March–April 2016, see also Krastel, 2016). The CIRCEE-HR seismic data were acquired using a 450 m long, 72 channel Sercel seismic streamer with an average geophone spacing of 6.25 m. The seismic source was a six mini-GI airgun array with a total volume of 111 cubic inches fired at a cadence of once every 6 s, for an average shot spacing of 16 m and a 24-fold coverage for each common midpoint. Quality control of the seismic data, including processing of the navigation files (shot position and streamer geometry), was performed with the SISPEED software (Ifremer). The seismic data were subsequently bandpass filtered (70–425 Hz), stacked, and time migrated (water velocity of 1500 m/s), using the Seismic Unix software package. During cruise POS496, an 80-channel digital solid-state Geometrics GeoEel streamer with a group interval of 1.5625 m was used for seismic acquisition. A Sercel Mini GI-Gun seismic source, with a total volume of 0.4 L, was shot in a harmonic mode. The shot interval was set to 6 s, resulting in a shot distance of ~12 m at a ship's speed of four knots. The seismic profiles were processed by using the commercial software package Schlumberger Vista Seismic Processing. The processing workflow includes bandpass filtering with corner

frequencies of 40/80/600/1000 Hz, despiking, debias filtering, CMP binning, and normal-move-out (NMO) correction. All data were time migrated by using the software's finite difference migration. Due to the relatively short streamer and the high water depths, no dedicated velocity analysis could be applied during NMO correction and migration. Hence, a constant velocity of 1500 m/s was applied. Moreover, other published seismic dataset (Argnani and Bonazzi, 2002; Argnani and Bonazzi, 2005; Argnani et al., 2012; Polonia et al., 2016; Polonia et al., 2017) and high-resolution bathymetry (Gutscher et al., 2016; Gutscher et al., 2017) were considered to better constraint the spatial extension of faults at the seafloor and their in-depth geometry.

Only the most representative seismic lines will be described in detail in this article (see *Deformation Pattern and Fault Activity*), whereas basic line drawing of the POS496 dataset (TWT) and of the entire time to depth-converted seismic dataset (including published seismic lines) can be found in the Supplementary Material (**Supplementary Figures 1 and 2**). To obtain geometric realistic parameters of the faults, seismic profiles (**Supplementary Figure 3A**) were time/depth converted by assigning average acoustic velocity to the two-way travel time sequence thickness (see *Seismic Stratigraphy*). The adopted acoustic velocity model was achieved from previous studies in the area (Gallais et al., 2011; Gross et al., 2016; Kokinou et al., 2013; Le Meur, 1997; Maeasano et al., 2017), and it is reported in **Supplementary Table 1**. Once time/depth converted, 2D linear features (fault traces and top/base reflectors) picked all along the seismic dataset (**Supplementary Figure 3B**) were modeled as 2½D features using common interpolation methods (e.g., kriging and IDW, **Supplementary Figure 3C**) operated into the Move 2019.1 geomodelling software package (Petex Ltd.). Bathymetric fault expression allowed us to further constrain the along-strike fault geometry (see **Supplementary Material**).

The local stress field orientation was derived by structural measurements performed on-land in the adjacent coastal sector. Structural data consist of mesofaults and fracture planes attitude and kinematic indicators mainly collected along the outcropping Miocene carbonate and Quaternary top sequences (see **Supplementary Table 2**). Even if the weak lithology (coarse sandstones, gravels, etc.) of Quaternary deposits does not usually favor the development or preservation of kinematic indicators, movement directions along faults planes have been obtained by tectogrooves, Riedel fractures, and rare slickenlines. All data were digitally stored on field by using Field Move Mobile App and finally analyzed and plotted using the FaultKin eight software (Allmendinger et al., 2012; Cardozo and Allmendinger, 2013) by adopting Schmidt's lower hemisphere projection.

Obtained stress field orientation was compared to other data concerning the modern deformation field at local and regional scales and finally applied on the 2½ D modeled fault surfaces to predict their tendency to the tectonic reactivation.
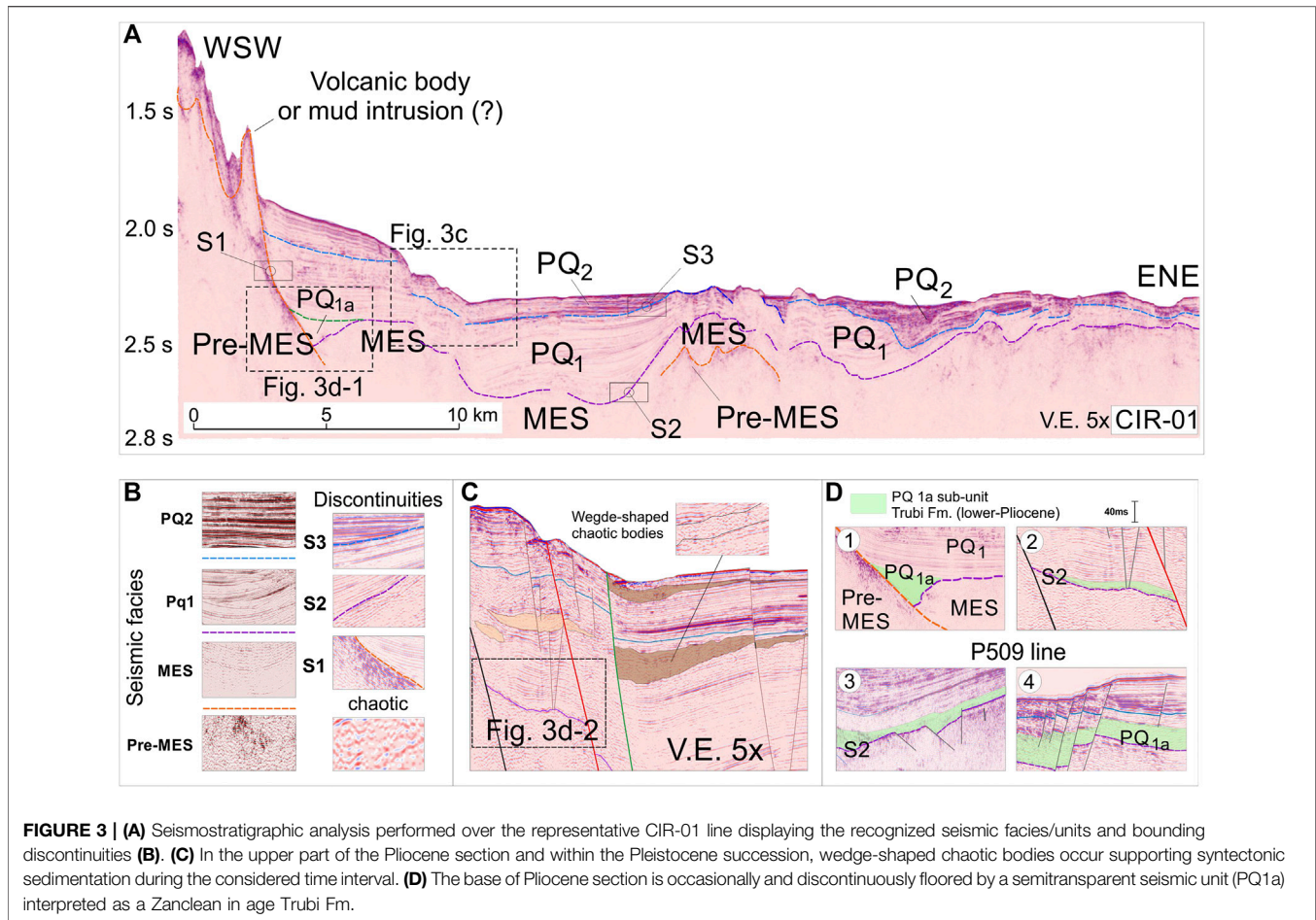
OFFSHORE GEOPHYSICAL DATA

Seismic Stratigraphy

Interpretation of seismic profiles allowed us to recognize four main seismic units based on i) their seismic features (e.g., amplitude, lateral continuity, and frequency of internal reflectors), ii) bounding discontinuities, and iii) strata architecture. Accordingly, basin-fill seismostratigraphic units were distinguished and labeled from older to younger as pre-MES, MES, and PQ, and the latter was furtherly subdivided into the subunits PQ_1 and PQ_2 (**Figure 3A**). The units are generally confined between well-defined discontinuities that have been interpreted as angular and/or erosional unconformities (S1, S2, and S3 in **Figure 3A**).

The pre-MES (acoustic basement) consists of a chaotic, locally transparent unit occasionally characterized by isolated and highly reflective bodies (**Figure 3B**). To the west, the seismic unit is truncated upward by an erosive surface (S1 in **Figure 3A**), a paleoslope above in which the younger units unconformably deposited, generally with on-lap and/or off-lap geometries (**Figure 3B**). The overlying MES unit is characterized by low- to medium-amplitude reflectors with medium frequency and locally subparallel geometry (**Figure 3B**). The unit is limited upwards by the S2 discontinuity (**Figure 3A**) that consists of an irregular erosive surface above which the overlying units often rest in paraconformity (**Figure 3B**). The PQ_1 unit consists of a variable in thickness alternance of low- to high-amplitude, low-medium frequency, subparallel or occasionally cross-stratified continuous reflectors (**Figure 3B**). Toward the west, along the MESC slope, the PQ_1 unit on-laps directly on the pre-MES unit, while upwards, it is delimited by the S3 discontinuity that is locally represented by an undulated erosive truncation. Close to the fault planes, the unit includes wedge-shaped seismic bodies with chaotic facies thinning away from the faults (**Figure 3C**). To the bottom, the PQ_1 unit is locally floored by a semitransparent seismic unit (subunit PQ_1a in **Figure 3A**) that, although discontinuously, was detected in most of seismic lines, where generally, it occurs within structural depressions or paleochannels (**Figure 3D**). The overlying PQ_2 unit is characterized by high-frequency, laterally continuous, parallel, and high-amplitude reflectors (**Figure 3B**). Locally, the PQ_2 unit on-laps against or down-laps on the older PQ_1 unit, and it is limited upwards by the seafloor.

In the absence of drill-hole data from the sediment section, we provide a basic lithological interpretation of the detected seismic units by following the available literature and by comparing the marine geophysical data with the on-land geology. The pre-MES unit is not well highlighted by the seismic signal, but locally its seismic features are consistent with carbonate-type sequences, a lithology widely outcropping on-land. Accordingly, the pre-MES unit has been interpreted as a Cenozoic sediment package that includes mainly limestone and marls, locally pierced by volcanic and/or mud intrusions forming sometimes cone-shaped seamounts at the seafloor (**Figure 3A**) (see also Scandone et al., 1981; Catalano et al., 2001; Barreca, 2014). According to its seismic characters (high reflectivity of the top reflector) and to the abundant literature concerning similar deposits occurring all around the Mediterranean basin (Lofi et al., 2011; Micallef et al., 2019 and references therein), the MES unit has been interpreted as Messinian in age deposits (mainly gypsum and evaporitic carbonate). The overlying Unit PQ_1 is interpreted as a part of the Pliocene succession since it correlates with the subunits "PQb"

FIGURE 3 | (A) Seismostratigraphic analysis performed over the representative CIR-01 line displaying the recognized seismic facies/units and bounding discontinuities **(B)**. **(C)** In the upper part of the Pliocene section and within the Pleistocene succession, wedge-shaped chaotic bodies occur supporting syntectonic sedimentation during the considered time interval. **(D)** The base of Pliocene section is occasionally and discontinuously floored by a semitransparent seismic unit (PQ1a) interpreted as a Zanclean in age Trubi Fm.

and "PQc" described by Camerlenghi et al. (2019) and partly with the "Unit one" of Micallef et al. (2018). The basal portion of this unit is locally characterized by the occurrence of a semitransparent body (PQ$_1$a in **Figure 3D**) that for its stratigraphic position is interpreted as the Zanclean in age Trubi formation (Butler et al., 2015). The seismic character of the PQ$_2$ unit suggests that it consists of a well-layered alternance of marly–arenaceous succession. Accordingly, PQ$_2$ unit can be interpreted as part of the Pleistocene sequence since it correlates for stratigraphic position and lithology with the distal part of the Panchina formation, outcropping on-land and characterized by Middle-Late Pleistocene sands and biocalcarenites (Servizio Geologico d'Italia, 2011). Moreover, it correlates with the PQa unit of Camerlenghi et al. (2019), whose basal erosional surface has been dated at 650 ka from DSDP site 374 cores (Hsü et al., 1978).

Deformation Pattern and Fault Activity

Displaced reflectors observed throughout the entire seismic dataset (**Supplementary Figure 1B**) and the analysis of the available bathymetric data (i.e., Gutscher et al., 2017 and Emodnet database) have allowed depicting the tectonic pattern that characterizes the northernmost sector of the Malta Escarpment. The recognized tectonic structures form an array

of sea-dipping, NNW–SSE trending, dip-slip faults extending offshore from Catania (in the north) to Siracusa (in the south) for a total length exceeding 60 km (**Figures 4** e-f). Within the system, three major faults segments (F1, F2, and F3 in **Figure 4A**) and minor faults (F4 and F5) have been structurally and geometrically characterized following their offsets in seismic lines and their bathymetric expression (see **Supplementary Material**). The F1 fault segment is the westernmost tectonic structure of the system and consists of an E-dipping, roughly N–S trending, 45 km-long, dip-slip fault. Following the seafloor expression, the F1 fault terminates against the NAF (North Alfeo Fault of Gutscher et al., 2016 or Alfeo–Etna Fault of Polonia et al., 2016, see **Figures 1A,C** for location) as suggested by cross-cutting relations. To the south, F1 merges to F3, the longest fault of the system. The fault has propagated throughout the illuminated subseafloor setting and has displaced the detected seismostratigraphic units with variable offsets (**Figure 4B**). According to the adopted time/depth conversion model (see **Supplementary Table 1** and *Offshore Geophysical Data*), F1 has displaced the base of the PQ$_1$ (S2 surface) and PQ$_2$ (S3 surface) units up to 460 and 260 m, respectively. Displacement has propagated up to the seafloor producing in average a vertical offset of about 70 m with a maximum value (about 150 m) along the MESC09 line. The F2 fault segment occurs about 2 km east of
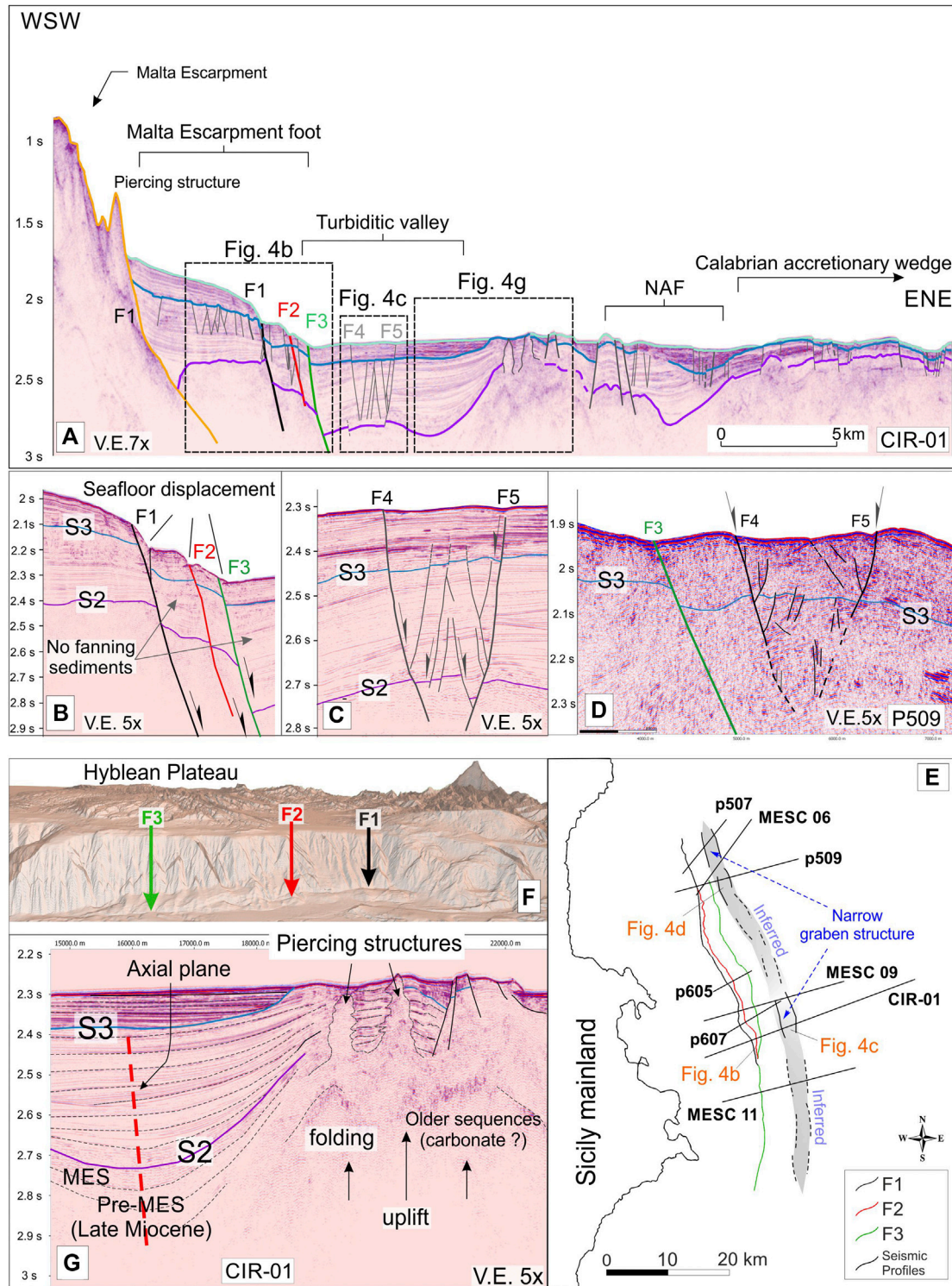
FIGURE 4 | (A) 3D perspective view of the interpreted seismic dataset. **(B)** Structural interpretation performed over the CIR-01 line showing the tectonic features occurring in the area. **(C)** Extensional E-dipping fault system deforming the foot of the Malta Escarpment and narrow graben structure propagating through the turbiditic valley recognized along the CIR-01 **(D)** and P509 **(E)** seismic lines. Structural interpretation on the whole seismic dataset (see **Supplementary Figure 2**) allows to map accurately faults in the E-Sicily offshore **(F)** also following their bathymetric expression **(G)**. **(H)** Folded and diapirically pierced structure occurring in the western portion of the CIR-01 line and sediment pattern on its western limb.

F1 and consists of an E-dipping, NNW-oriented, 34 km-long fault structure. To the north, F2 converges toward F1, whereas to the south toward F3 (**Figure 4E**). This array suggests F2 as a subordinated splay fault. Fault activity has produced in average displacement in the S2 surface (MES top reflector) of about 150 m and in the S3 surface (PQ1 top reflector) of about 65 m, whereas seafloor appears to be displaced in average of about 30 m (**Figure 4B**). The F3 fault segment is the easternmost structure of the system controlling the foot of the MESC. The structure consists of an E-dipping, NNW trending fault with a total length of about 57 km. It has deformed the whole illuminated seismostratigraphic succession, displacing in average the S2 and S3 discontinuities of about 150 and 47 m, respectively (**Figures 4B,D**). Further east, a narrow (about 3.5 km wide) graben structure deforms the abyssal plain occupied by a 7 km-wide, N–S-oriented, sedimentary basin (turbidic valley of Gutscher et al., 2016, see **Figure 4A**). The graben structure roughly extends from the CIR-01 line, in the South (see **Figure 2** for location), to the Catania offshore, in the north, whereas its continuation further south has been only inferred because of lack of good quality seismic lines (see **Figure 4E**). It is bounded by opposite-dipping normal faults (F4 and F5 in **Figure 4A**), both characterized by a moderate offset gradually increasing with depth (**Figures 4C–D**). Diffuse minor splays associated with the major bounding faults internally deform the down-faulted block. The interpreted seismic dataset (see **Supplementary Figures 1 and 2**) revealed the continuity of the detected faults all along the offshore E Sicily, allowing to map accurately their spatial distribution (**Figure 4E**) and to follow their bathymetric expression at the seafloor (**Figure 4F**).
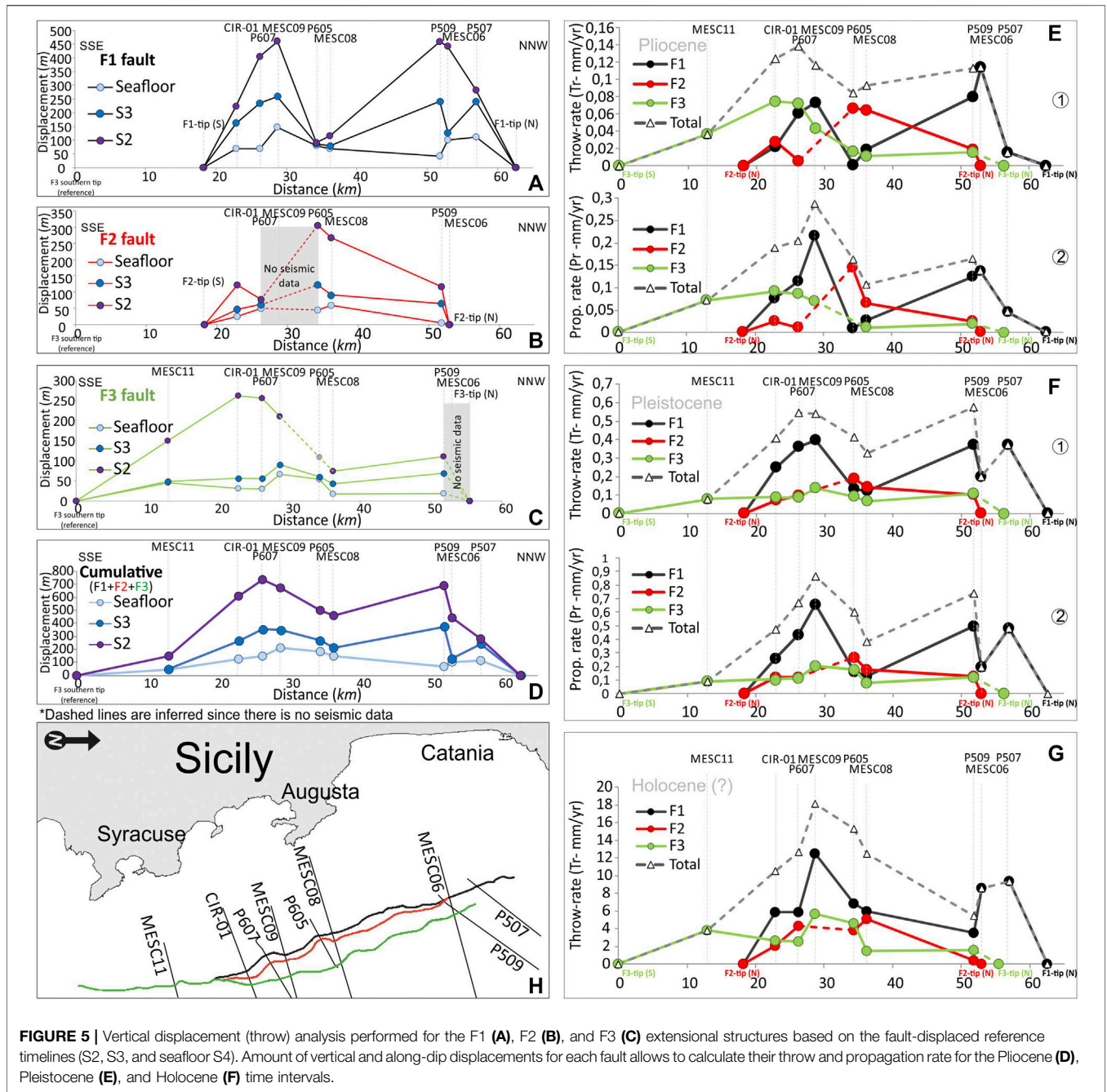
It is worth noting that a prominent structural culmination occurs to the east of the analyzed fault system, bounding the turbiditic valley (the uplifted area of Argnani and Bonazzi, 2005). It consists of ~10 km-wide folded sectors interpreted as a positive flower structure related to the recent activity of the North Alfeo Fault System by Gutscher et al. (2016) or as a forced fold related to the upraise of a mantle-derived serpentinite diapirs by Polonia et al. (2017). Seismostratigraphy and growth geometry on the limbs of the folded structure suggests that it was active from the Late Miocene up to the Late Pliocene before being eroded on its top (S3 discontinuity), sealed by Pleistocene sediments, and it was finally pierced by some diapiric structures (**Figure 4G**). Accordingly, the time-growing of the folds indicates that they cannot be related to the recent activity of the North Alfeo Fault nor (as proposed by Argnani and Bonazzi, 2002; Argnani and Bonazzi, 2005) to the tectonic shortening of the deformation front of the Calabrian accretionary wedge since it was located far away (>100 km) to the NW during the Late Miocene–Pliocene. In this frame, most of the diverging pattern of the upper Miocene–Pliocene strata is interpreted as related to the time-growing uplifting of the fold system rather than to the Quaternary activity of North Alfeo and/or MESC faults, accounting thereby for a more recent onset of the extensional deformation in the area. The occurrence of some wedge-shaped, chaotic seismic bodies thinning away from the faults mainly within the PQ2 unit (see *Seismic Stratigraphy* and **Figure 3C**) along with the very slight sediment thickening observed close to the F1, F2, and F3 faults in

the older sections (**Figure 4B**) support, in fact, the initiation of extensional tectonic activity around the Early Pleistocene. During this period, slight fanning strata and the nondevelopment of a typical sedimentary wedge opening toward the faults should be charged to the consistent rate of sedimentation (about 0.4 mm/yr) characterizing the Pliocene section that was higher than the tectonic rate of the three extensional faults (<0.1 mm/yr, see *Deformation Pattern and Fault Activity*).

Fault Displacement Analysis and Deformation Rate

With the aim of estimating the deformation rate of tectonic structures characterizing the MESC, a fault displacement analysis was performed on the time/depth-converted seismic dataset (see **Supplementary Figure 2**). The displacement produced by the activity of the main detected faults (F1, F2, and F3) was measured considering the vertical component (throw) and using fault-displaced reference timelines (S2, S3, and S4-seafloor, see **Supplementary Table 3**). Throws measured along each fault for the S2 (top-MES), S3 (top-PQ1), and the seafloor describe in general an along-strike variable pattern with displacements decreasing from the fault center to the tips (**Figure 5**). Longitudinal trends for F1 and F2 faults define a double bell-shaped pattern for the three displaced timelines with relative maxima of throw (about 460 and 300 m, respectively) recorded by the older F1-displaced S2 surface, whereas the younger S3 is less deformed by the same fault as it reaches the maximum offset of about 260 m (**Figures 5A,B**). By contrast, longitudinal throw trend of the F3 structure outlines a double bell-shaped pattern only for the older S2 surface, whereas S3 and the seafloor timelines (S4) tend to assume an irregular pattern resembling a single bell-shaped throw curve (**Figure 5B**). Displacement of the seafloor was analyzed to evaluate the recent deformation history of the detected faults even if a large uncertainty could affect offset estimation, related to the erosive or depositional nature of the seafloor. Nonetheless, the along-strike trend of the seafloor throw produced by the considered faults displays different patterns varying from a double bell-shaped curve for the F1 structure (**Figure 5A**) to a single bell-shaped curve for the F2 and F3 structures (**Figure 5C**). The recent and combined activity of the faults has produced a cumulative offset at the seafloor of ~210 m.

Based on the vertical and along-dip offsets measured on the displaced S2 (top-MES), S3 (top-PQ$_1$), and on the seafloor (S4) reference timelines and considering time intervals for the fault-deformed sections PQ1 (Pliocene, 2.75 Myr), PQ2 (Middle-Upper Pleistocene, 0.63 Myr, see *Seismic Stratigraphy*), and ~Holocene (0.0117 Myr), the long- and short-term throw (T_r) and propagation rates (P_r) for the three main faults have been estimated (**Figures 5E,F,G**). Accordingly, measured vertical (T_r) and along-dip (P_r) displacement components were restored at the considered time interval by removing from the cumulated older offsets the contribution of the younger fault movement. During the Pliocene, faults slipped simultaneously but with different rates according to the measured two-component of movement, in average higher for the F1 ($T_R \sim 0.05$ mm/yr and $P_R \sim 0.09$ mm/yr) and lower for the F2 ($T_R \sim 0.04$ mm/yr and $P_R \sim$

FIGURE 5 | Vertical displacement (throw) analysis performed for the F1 **(A)**, F2 **(B)**, and F3 **(C)** extensional structures based on the fault-displaced reference timelines (S2, S3, and seafloor S4). Amount of vertical and along-dip displacements for each fault allows to calculate their throw and propagation rate for the Pliocene **(D)**, Pleistocene **(E)**, and Holocene **(F)** time intervals.

0.05 mm/yr) and F3 (T_R~ 0.04 mm/yr and P_R ~0.06 mm/yr), respectively (**Figures 5E1–2** and **Supplementary Table 4**). Since the Middle Pleistocene, faults accelerated slipping at a higher rate compared to the Pliocene. During this time interval, the F1 still slipped faster (in average T_R~ 0.27 and P_R~0.4 mm/yr) than the F2 (in average T_R~ 0.12 and P_R~0.16 mm/yr) and F3 (in average T_R~ 0.04 and P_R~ 0.12 mm/yr), respectively (**Figure 5F**). In this stage, the segmented F1 and F2 evolved (fault linkage) in well-defined structures. The poorly constrained Holocene deformation pointed out a further acceleration of the faults

during this time interval even if, as stated above, large uncertainties (erosion, slope instability, etc.) could affect bathymetric throw measurements. T_R for F1 and F2 reaches in average the value of ~7.3 and 3.1 mm/yr, respectively, whereas about 3.2 mm/yr has been calculated for the F3 structure (**Figure 5G**). The high throw rate value calculated for the F1 suggests that this value could be amplified by a nontectonic component. Conversely, throw rates for F2 and F3 are consistent with tectonic deformation and coherent with the return periods for large earthquakes in the area (see *Discussion*).
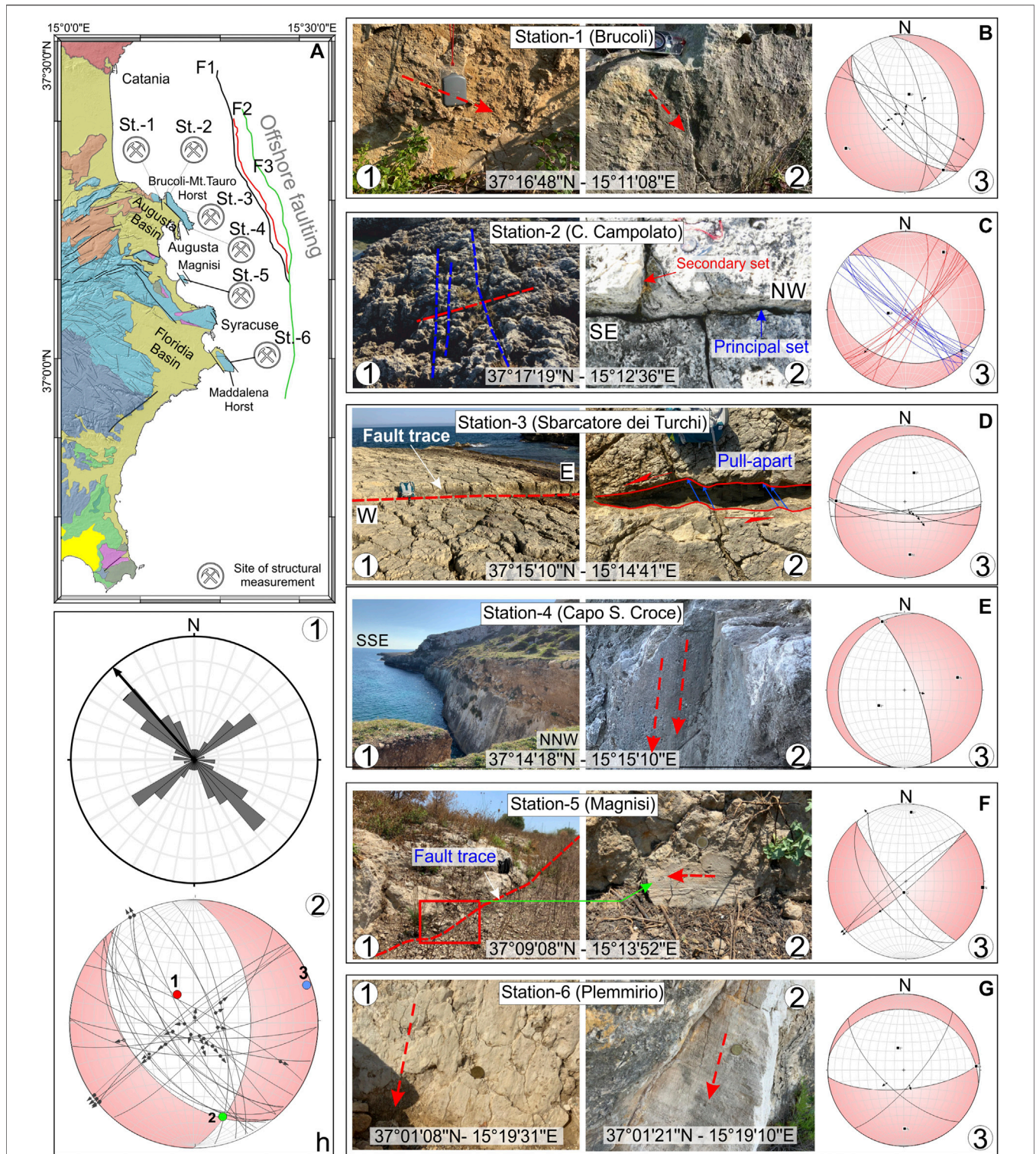
FIGURE 6 | (A) Location of the sites of structural measurements performed along the footwall block of the Malta Escarpment (SE Sicily coastal domain, see Figure 1B for the geology on-land) and collected fault planes and kinematic indicators (B–G). Diagrams on the right panels (Schmidt lower hemisphere) show faults plane attitude and movement on the respective hanging walls (black arrows) and calculated pseudofocal mechanisms. h-1) Rose diagram of the whole mesostructural dataset showing the faults having a dominant strike in the range N130–140E. h-2) Stress field derived from slip-data inversion highlighting the area as deformed under a slightly transtensional tectonic regime characterized by a ~70° plunging, NNW–SSE trending σmax.

ON-LAND STRUCTURAL DATA

To derive the orientation of the local stress field, geostructural data were collected in six key sites along the Hyblean coastal domain, between the cities of Augusta and Syracuse, on the footwall block of the offshore faults that were analyzed (**Figure 6A**). According to available geological maps (Carbone et al., 1984; Carbone et al., 1986; Servizio Geologico d'Italia, 2011), in this area Lower-Middle Miocene carbonates mostly outcrop, unconformably covered by a regressive Quaternary sequence made up of marly-clays, sands, and calcarenites. The investigated sector has been deformed by an array of NNW–SSE trending and dip-slip/oblique faults (**Figure 6A**) whose activity has produced horst (i.e., Brucoli–Mt. Tauro, Magnisi, and Maddalena) and graben (i.e., Augusta and Floridia Basins) structural associations whose bounding structures are roughly coaxial to the faults detected in the offshore (see *Deformation Pattern and Fault Activity* and **Figure 6A** for location).

Faults and Fractures

Along the Brucoli–Mt. Tauro horst structure, in the North (**Figure 6A**), Miocene and Quaternary deposits have been mainly deformed by oblique faults systems and associated fracturing. In the Brucoli area (Station-1, **Figure 6A**), mesostructures mostly consist of subvertical (70–80° dipping) NNW–SSE and NW–SE trending fault segments. Kinematic indicators (slickenlines and rare tectogrooves, see **Figure 6B**), suggest oblique right-lateral and dip-slip movement and a rare left-lateral component on the NNW–SSE and NW–SE-oriented fault planes, respectively (see diagram in **Figure 6B**). At the Capo Campolato locality, in the northern termination of the Mt. Tauro–Brucoli structural culmination (station-2, **Figure 6A**), outcropping carbonates are pervasively deformed by a system of extensional cross-joints (**Figure 6C**). The system is arranged in a ladder-like geometry with a more continuous and principal joint-set-oriented NW–SE and a secondary one oriented orthogonally according to the NE–SW direction (see diagram in **Figure 6C**). At Sbarcatore dei Turchi (station-3, **Figure 6A**), a system of south-dipping, roughly E–W striking fault planes has been measured (**Figures 6D–L**). Sense of movement on fault planes was derived by dislocated geological markers exposed on both sides of the structures. The reconstructed vertical and lateral component of movement (resulting slip-vector plunging toward the SE at 60–80°) and alongside pull-apart basins (**Figure 6D**) suggest oblique, left-lateral kinematics for the detected fault planes (see diagram in **Figure 6D**). At Capo S. Croce locality (station-4, **Figure 6A**) in the southernmost termination of the Mt. Tauro–Brucoli horst, structural measurements were performed on the eastern border fault. The structure is well exposed along the coastline where it forms a subvertical sea cliff (**Figures 6E–L**) and consists of an ENE-dipping, NNW–SSE trending fault. Slickensides on fault plane dipping at 70° toward the N65E direction (**Figures 6E-2**) indicate an extensional dip-slip sense of movement according to an ENE trending extension (see diagram in **Figure 6E-3**). Further south, data were collected along the Magnisi Peninsula (station-5, **Figure 6A), a** narrow carbonate horst bounded by NNW–SSE trending faults

(**Figure 6F**). Slickensides on mesostructures planes were collected on the landward side of the peninsula where strike-slip faults with related pull-apart basins and associated fractures occur (**Figure 6F**). The few kinematic indicators suggest a right-lateral sense of movement for the detected faults (see diagram in **Figure 6F**). Some data have also been collected along the Maddalena horst south of Syracuse (station-6, **Figure 6A**) which consists of NW–SE and NE–SW trending oblique right-lateral transtensional mesofaults (**Figure 6G**).

Stress Field

The paleostress tensors for the onland faults were derived by using directional statistics (e.g., Linked Bingham Analysis, Bingham, 1974) that is based primarily on the slip-data inversion of fault planes exhibiting clear kinematic indicators. Extensional joints pattern measured at the station two were included, considering that, in a ladder-like joint arrangement, the orientation of the principal joints-set (the more continuous, **Figure 6C**) coincide with that of the maximum stress axis (Bai and Pollard, 2000; Bai et al., 2002). Data analysis revealed that the on-land area has been deformed by an array of slightly (right-lateral) oblique faults oriented in a prevailing NNW–SSE direction (18.75% between N131 and 140E, see rose diagram in **Figure 6H**) developed under a stress field characterized by a 70° plunging, nearly N–S-oriented (N330E) σ max and by a subhorizontal, about E–W oriented σmin (**Figure 6H**). Slip-data inversion also provides a pseudofocal mechanism which is characterized by a P-axis plunging toward N332E at about 70° and by a subhorizontal T-axis-oriented N70E (**Figure 6H**). Although field measurements and slip-data inversion point to the on-land faults being deformed under a slight transtensional tectonics regime, the propagation of the tectonic structures through the Quaternary sequences remains doubtful; accordingly, the age of last deformation events is not fully determinable. Despite this, the comparison of our results with other published data concerning stress tensors at local and regional scales suggests that the derived stress field is compatible with the recent kinematic of SE Sicily. In fact, computed ENE–WSW trending σmin is roughly consistent with i) the regional NE–SW to WNW–ESE extension derived from inversion of slickensides data on fault planes (Adam et al., 2000; Monaco and Tortorici, 2000; De Guidi et al., 2013), ii) geodetic data (D'Agostino and Selvaggi, 2004; Mattia et al., 2012; Palano et al., 2012), and iii) the local ENE–WSW trending minimum stress resulting from boreholes breakout data analysis in the eastern sector of the Hyblean Plateau (Ragg et al., 1999; Montone et al., 2012).

FAULT MODELING AND SEISMOTECTONIC POTENTIAL

Structural interpretation and interpolation of 2D seismic profiles and time/depth conversion of seismic dataset along with faults bathymetric expression (see *Deformation Pattern and Fault Activity* and **Supplementary Table 1** for adopted velocity model) allowed us to build up a simplified but consistent
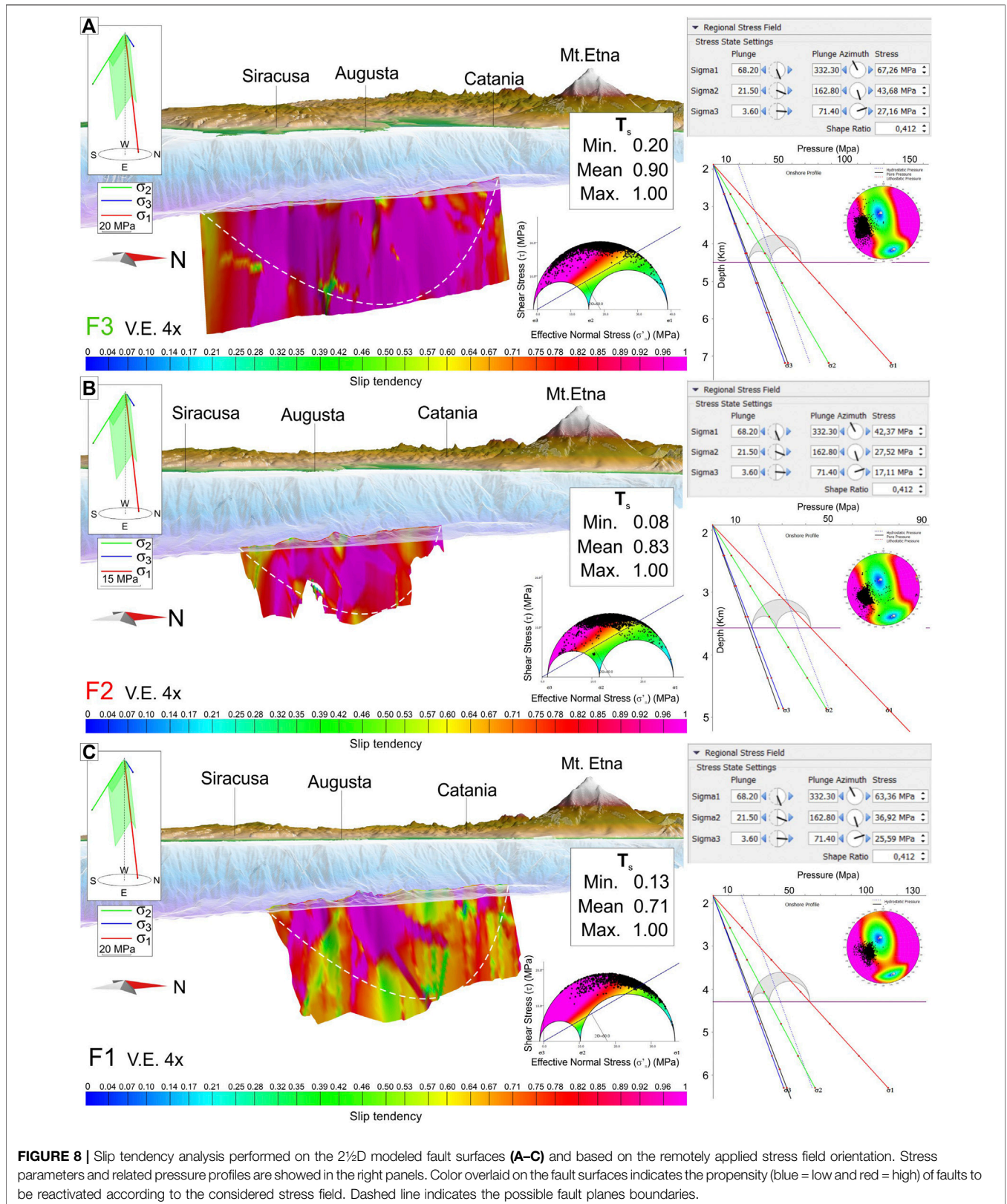
FIGURE 7 | (A) 2½D fault surfaces (perspective view from the SE) modeled according to reference lines (fault traces) picked along the seismic dataset (see **Supplementary Figure 1** for the workflow) and related attitude in the 3D environment **(B)**.

TABLE 1 | Geometric parameters derived from the 2½D data modeling and expected magnitudes from empirical-scaling relationships (Wells and Coppersmith, 1994; Leonard, 2010). Note that, according to fault segmentation inferred from the fault displacement analysis (see *Fault Displacement Analysis and Deformation Rate*), seismic potential for F1 and F2 faults may be overestimated.

Geometric parameters		F1				F2				F3	
Mean strike		**N345E**				**N340E**				**N352E**	
Mean dip (°)		**36**				**46**				**49**	
Length (km)		**44.44**				**33.72**				**56.46**	
Fault depth range and width (m)	min	**Width***	Max*	min	**Width***	Max*	min	**Width***	Max*
	−1,813	**4,337**	−6,150.5	−1908	**3,322**	−5,230	−1854	**5,275**	−7,129
Area (km²)*		276.92				98.65				334.05	
				Expected magnitude, Wells and Coppermisth (1994)							
	min	*mean*	*max*	*min*	*mean*	*max*	*min*	*mean*	*max*
M based on surface rupture length (SRL)	6.27	**7.03**	7.80	6.14	**6.88**	7.61	6.38	**7.17**	7.97
M based on rupture area (RA)*	5.95	**6.42**	6.90	5.53	**5.96**	6.39	6.02	**6.50**	6.99
M based on downdip rupture width (RW)*	6.27	**7.04**	7.81	6.15	**6.89**	7.63	6.38	**7.17**	7.97
				(*) underestimated							
				Expected magnitude, Leonard (2010)							
M based on surface rupture length (SRL)		**6.99**				**6.79**				**7.16**	
M based on rupture area (RA)*		**6.44**				**5.99**				**6.5**	
% difference WC94-L10 on SRL		**0.54**				**1.23**				**0.09**	
% difference WC94-L10 on RA		**0.32**				**0.5**				**0.3**	

2½D model of the faults occurring in the study area (**Figure 7A**, see also **Supplementary Figure 3** for the workflow). Although depth-limited, due to the penetration of the seismic signal in the subseafloor, the model provides an estimate of the geometric parameters (i.e., length, width, dipping, and strike, see **Figure 7B** and **Table 1**) for the shallow portion of the investigated faults.

According to the reconstructed model and to the fault displacement analysis, the F1 consists of a roughly 45 km-long, two-branched structure-oriented N345E with a fault plane dipping toward the ENE at about 45°. The F2 is a N340E trending two-branched structure, about 35 km-long dipping at 50° toward the ENE. Finally, F3 is a continuous,

FIGURE 8 | Slip tendency analysis performed on the 2½D modeled fault surfaces **(A–C)** and based on the remotely applied stress field orientation. Stress parameters and related pressure profiles are showed in the right panels. Color overlaid on the fault surfaces indicates the propensity (blue = low and red = high) of faults to be reactivated according to the considered stress field. Dashed line indicates the possible fault planes boundaries.

TABLE 2 | Deviatoric stress applied to the modeled fault surfaces and considered elastic parameters of the medium.

Fault	σ1 Magnitude (Mpa)	σ1 Azimuth (°)	σ1 Dip (°)	σ2 Magnitude (Mpa)	σ2 Azimuth (°)	σ2 Dip (°)	σ3 Magnitude (Mpa)	σ3 Azimuth (°)	σ3 Dip (°)	Pore pressure (Mpa)	Cohesion (Mpa)	Friction angle (°)	Young's modulus (Mpa)	Poisson's ratio	Friction coeff.
F1	63.4	332.3	68.2	36.9	162.8	21.5	25.6	71.4	3.6	26.7	0	30	27,000	0.25	0.58
F2	42.4	332.3	68.2	27.5	162.8	21.5	17.1	71.4	3.6	16	0	30			
F3	67.3	332.3	68.2	43.7	162.8	21.5	27.2	71.4	3.6	28.3	0	30			

roughly 60 km-long fault with a N352E-oriented fault plane dipping toward the east at 55° (see pole/attitude diagrams in **Figure 7B** and **Table 1**). Derived fault geometric parameters were then used as input data to estimate the maximum expected earthquake magnitude for each fault assuming a reactivation where there is a seismic slip along their entire length. Based on the surface rupture length (SRL) and the underestimated rupture area (RA) and considering fault segmentation (i.e., for F1 and F2, see **section 4.3**), empirical scaling relationships (Wells and Coppersmith, 1994; Leonard, 2010) put forward a high seismic potential for the most continuous F3 faults capable of generating events exceeding magnitude 7 (see also Trippetta et al., 2019). (**Table 1**). Even if fault reactivation depends on several parameters such us surface frictional characteristics, fault cohesion, shear normal stresses on the fault plane, and fluid pressure, potential reactivation of faults has been here evaluated through a slip tendency analysis (Morris et al., 1996), which defines the propensity of a surface to undergo slip when a stress is applied. Slip tendency (T_s) is based on Amonton's law which governs the slip of a cohesionless plane and is expressed by the shear/normal stress ratio acting on the surface (Morris et al., 1996). The formulation is

$$Ts = \tau/\sigma'n,$$

where τ is the shear stress and σ'_n is the effective normal stress (i.e., the normal stress minus fluid pressure) acting on the plane. Following the assumptions proposed in the Wallace–Bott hypothesis (Wallace, 1951; Bott, 1959) and using the stress analysis tools of Move 2019.1 software (Petex Ltd.), stress field tensors orientation derived from slip-data inversion (see *Stress Field*) were remotely applied to the modeled fault surfaces (**Figure 7**). Considering an average density of 2,600 and 1050 kg/m³ for the overburden rocks and seawater, respectively, and approximating the maximum stress (σ_1) to the lithostatic load, a confining stress is resolved at a mean depth in the medium around each fault (see applied stress and relative pressure profiles for each fault in **Figure 8** right panels and in **Table 2**). Slip tendency computation (T_s in **Figure 8**) found that the F3 as the fault structure most prone to be reactivated along its entire length with the highest average T_s value (0.90) homogeneously distributed along the fault plane (**Figure 8A**). F2 also exhibits a high mean T_s value of 0.83 with a maxima ($T_s = 1$) reached mainly on the southern portion of the fault plane (**Figure 8B**). Conversely, F1 shows the lowest average T_s value (0.71) with a maxima ($T_s = 1$) occurring over limited and shallow portions of the fault plane mainly off Siracusa and Augusta (**Figure 8C**). Additionally, the fault displacement analysis (see *Fault Displacement Analysis and Deformation Rate*) suggests segmentation of the F1 and F2 faults (i.e., the double bell-shaped displacement pattern, see **Figure 5C**), suggesting these structures have grown following a segment linkage pattern. Accordingly, a lower seismic potential should therefore be applied to these tectonic structures. Conversely, fault displacement analysis revealed that the F3 fault structure has grown in a radial way since at least the Pleistocene whereby its seismic potential has likely not been overestimated.

DISCUSSION

Structural interpretation of seismic reflection data on the Ionian Sea offshore of SE Sicily, field measurements, and 2½D data modeling provide further information on the tectonic pattern and deformation rates affecting the northernmost sector of the Malta Escarpment since the Pliocene times. Seismic data illuminates, with good resolution, the shallowest portion of some of the tectonic structures previously mapped in the area (e.g., Bianca et al., 1999; Argnani and Bonazzi, 2002; Argnani and Bonazzi, 2005; Argnani et al., 2012; Polonia et al., 2012; Gutscher et al., 2016; Maesano et al., 2020) providing an opportunity to better characterize their dimension and through-time tectonic activity. These data reveal that deformation in the Ionian Sea offshore of SE Sicily is accommodated by a nearly N–S trending fault belt that is composed of three main, E-dipping, and slightly oblique (right-lateral) fault segments (F1, F2, and F3 in **Figure 4**). Seismostratigraphic pattern analysis within the recognized seismic units was performed to achieve information on fault activity. However, the growth of the fold and thrust system located to the east of the investigated faults and the thickening of late Miocene–Pliocene sediment on its flanks (**Figure 4H**) has posed significant issues in discerning inception of the extensional phase in the area. Dipping toward the culmination of the axial plane of the fold deforming the late Miocene–Pliocene sediment wedge in the turbiditic valley (see **Figure 4H**) allows excluding that fanning and folding of the strata could be generated by a sedimentary draping process. Accordingly, even though the geometry of the sedimentary wedge could be associated with the Quaternary activity of the extensional faulting to the west, we attribute the growth strata pattern of Upper Miocene–Pliocene sediments mostly to the trough-time uplift of folded system. This interpretation accounts for a possible more recent onset of the extensional deformation reactivation of the northernmost sector of the Malta Escarpment.

Fault deformation rates point out the investigated area as a slow-rate extensional domain where fault activity was modulated through time. The longitudinal fault-throw trend and the through-time deformation rate provide further information on the inception of extensional tectonics in the area and on the growing mode of the faults. According to the along fault strain localization over time, the very low deformation rate affecting the faults during the Pliocene strongly confirms the onset of extensional deformation since that time (see *Seismic Stratigraphy*), hence simultaneously to the growing of the folded system eastwards (see above). The observed bell-shaped pattern on the longitudinal fault-throw trend reveals that F1 and F2 faults have grown discontinuously in the Pliocene and suggest that they are probably segmented into two branches (**Figures 5E–F**). Consequently, each of these faults appears to have grown in the near-surface mainly by segment linkage rather than in a radial way (see Cartwright et al., 1995 for further explanation) even if no overlapping setting and relay ramps have been resolved at the seafloor where their vertical offset decreases considerably. Fault segmentation pattern seems also to have characterized the F3 fault activity only during the Pliocene, whereas since the Pleistocene, this fault has grown in a radial way working as a

continuous structure (**Figures 5E–F**). The increasing dip of the faults from west to east (36°, 46°, and 49°, respectively, for F1, F2, and F3, see **Table 1**) would suggest a rotational (simple shear) dominostyle deformation context where block-bounding faults, as the effect of rotation, become progressively unfavourably oriented to the maximum stress axis and new high-angle faults form. However, the simultaneous activity observed with the fault displacement analysis (see *Deformation Pattern and Fault Activity*) leads to interpret such faults as merging down-dip into a single tectonic structure even if depth penetration of seismic data does not resolve its deeper trajectory. Detected faults should be therefore thought of as low hierarchical-order splay structures through which the strain accumulated by the deeper and larger tectonic structure is partitioned at a shallow crustal level. Strain partitioning in the upper crust appears to be supported by the along-strike trend of displacements and throw rates (**Figure 5**).

By comparing the depicted tectonic pattern with other structural settings concerning passive margin worldwide (e.g., along the Pará-Maranhão Basin in the Brazilian equatorial margin, see Matos, 2000) and considering i) the long-lived (late Miocene–Pliocene) grown of the folds system, ii) its inferred simultaneous activity, during the Pliocene, with the extensional faults, iii) the high-rate of extensional deformation during the Holocene (in average about 5 mm/yr for the F1 and F2 structures, see **Figure 5G**) and iv) the low-angle and down-dip converging geometry of the F1, F2, and F3 faults, part of the observed deformations should be also charged to large-scale slope instability. According to this last hypothesis, both faults to the west and the fold to the east may have been initially nucleated by gravitational forces in a deep-seated gravitational slope deformation context. Later, in Quaternary times, a tectonic component of deformation probably prevailed as testified by the occurrence on the MESC footwall block (SE Sicily coastal domain) of a flight of out-of-water, Middle-Late Pleistocene marine terraces (Bianca et al., 1999), by oblique deformation on-land, and by the quite rectilinear fault traces at the seafloor. In this perspective, previous extensional faults related to the deep-seated gravitational slope deformation were obliquely reactivated since the Middle Pleistocene according to the E–W trending extensional kinematics resulting from regional-scale diverging motion affecting the lower plate of the collisional system (see **Figure 1A**).

Seismotectonic Implications

Whatever the process by which the normal faults were generated, earthquakes occurring in the area reveal that a seismogenic stress is anyway accumulating in the Western Ionian Basin at crustal level (see Musumeci et al., 2014). In this frame, considering that splays fall into an area, the SE Sicily, hit by large historical earthquakes (e.g., January 11, 1693, event with M = 7.4, Rovida et al., 2016), we estimated their seismic potential using empirical scaling relationships (Wells and Coppersmith, 1994; Leonard, 2010) and slip tendency analysis (Morris et al., 1996). Our combined analysis puts forward that the splays could be capable of generating high-energetic seismic events (see **Table 2**) and, among them, the longest and most continuous F3 fault could
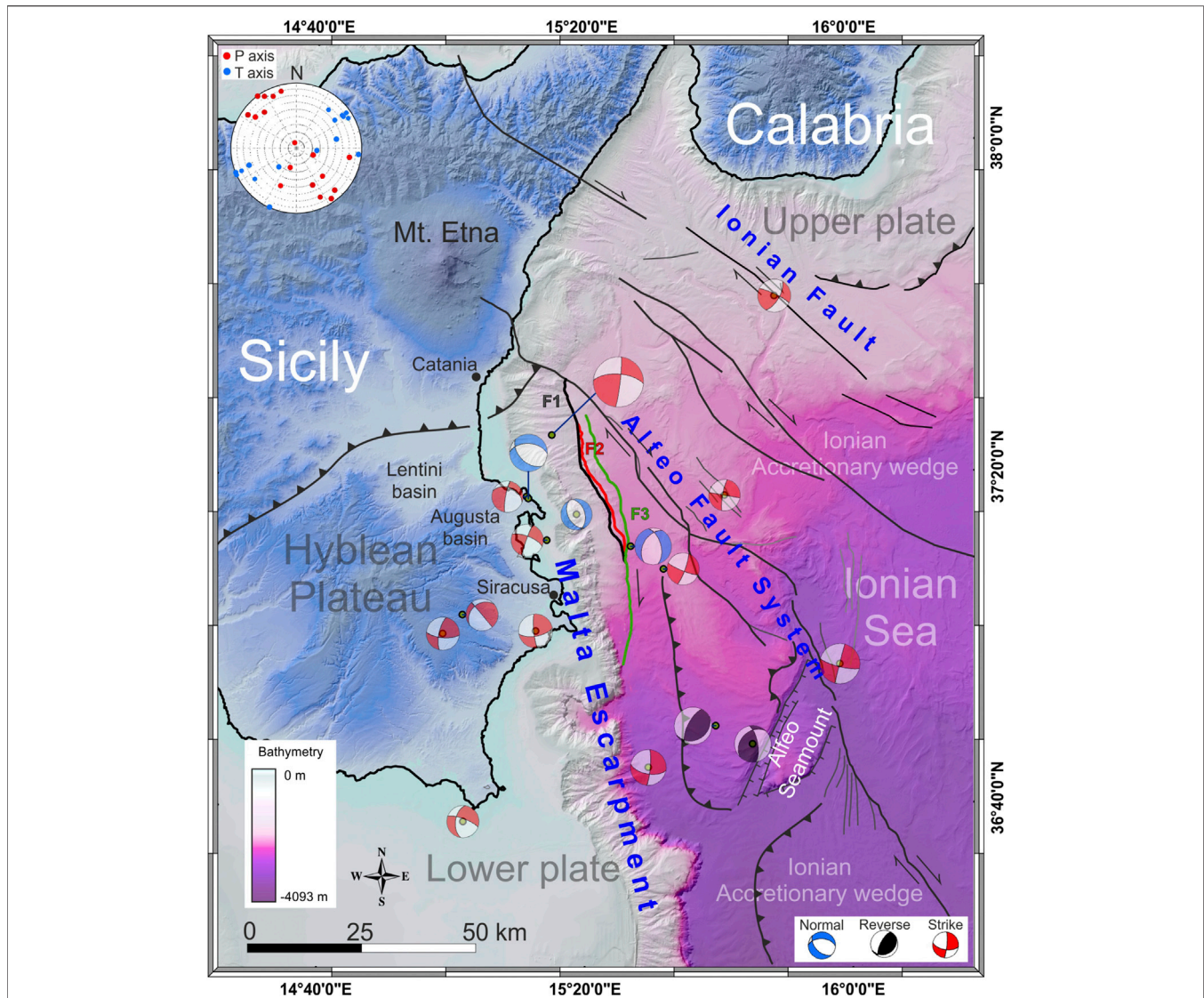
FIGURE 9 | Mapped faults (F1, F2, and F3) framed in the larger tectonic framework of the Western Ionian Basin. Alfeo Fault system and Ionian Fault are from Gutscher et al. (2016) and Polonia et al. (2016). Available focal solutions of M > 3.5 earthquakes (Pondrelli, 2002; Scarfi et al., 2013; Musumeci et al., 2014; Scarfi et al., 2016) and PT axes computation (see diagram in the top-left) support transtensional deformation in the studied area.

be the most prone structure to reactivation along its entire length which could therefore produce an earthquake exceeding magnitude 7. According to the empirical fault-scaling relationships (Wells and Coppersmith, 1994; Leonard, 2010), a 7.17 magnitude event expected for the F3 (see **Table 2**) would produce a maximum displacement (MD) of about 3 m or an average displacement (AD) of about 1.2 m. Assuming that the F3 seafloor scarp is the result of cumulative coseismic slips, the number of seismic events with M = 7.17 needed to produce such fault-scarp has been tentatively estimated by dividing the fault-scarp height for the coseismic displacement expected for 7.17 magnitude earthquakes (see **Table 2**). Furthermore, by dividing the age inferred for the S4 boundary (the seafloor) for the obtained number of seismic events (about 22 events considering the max throw/MD or about 25 seismic events

considering the mean throw/AD), a return period for large earthquakes (M > 7) can be estimated over the considered time interval. On this basis, given the height of the F3 fault-scarp at the seafloor (mean and max throw of 66 and 29 m, respectively, see **Figure 5C** and **Supplementary Table 3B**) and the inferred age for S4 (11.7 ka), the return periods of 470 years (considering the mean throw and the average expected displacement) and 537 years (considering the maximum throw and the maximum expected displacement), have therefore been estimated. It is worth to note that our estimation is quite close to the return periods provided by previous authors (e.g., Barbano et al., 2001; Bianca et al., 1999) for the studied area. Based on the inferred macroseismic intensity for historical earthquakes that have occurred in the Hyblean Plateau, Barbano et al. (2001) estimated indeed return periods of about 475 years for events

with intensity IX-X and 644 years for events with intensity X, even though the latter is associated with an extremely high error. Expected magnitudes and the estimated recurrence time interval are compatible with those inferred for large historical earthquakes in the area (e.g., the 1693 and 1169 events, see Barbano, 1985; Boschi et al., 1995; Rovida et al., 2016), suggesting the F3 fault the potentially causative faults from which destructive seismic events generated. This assertion appears to be supported for instance by the intensity contours of the 1693 event macroseismic field (see Barbano, 1985), suggesting an offshore seismic source since they are open to the Ionian Sea. The mismatch between the NNW orientation of the studied faults and the NE–SW trending of the macroseismic high-intensity contours should be explained by considering site effects according to which damages may have concentrated on-shore in areas where soft sediments outcrop (i.e., in the Augusta and Lentini basins, see **Figure 1C** and **Figure 9**). Furthermore, the prevailing dip-slip kinematic of the studied faults is in favor of producing tsunamis by coseismic seafloor displacement even if slope failure triggered by seismic shacking cannot be ruled out along the steep, 3,000 m high bathymetric drops of the Malta Escarpment (see Billi et al., 2010).

CONCLUSION

Seismic data interpretation from the offshore SE Sicily along with fault-applied empirical scaling relationships and forward methods allow is to achieve additional information on the structural pattern and seimotectonics of the northernmost branch of the Malta Escarpment. Primary findings are summarized as follows:

- The northernmost branch of the Malta Escarpment has been deformed recently according to E–W tectonic extension, and this kinematics appears to affect mainly the lower plate of the collisional system, whereas eastwards of the studied area, strike-slip deformation prevails within the Ionian accretionary wedge in the tectonically overlaying upper plate (see **Figure 9**).
- The occurrence of extension and contraction at the same structural level (see *Deformation Pattern and Fault Activity*) suggests that, during the Pliocene, faulting and folding may have been nucleated in response to the same process. By similarity with the structural settings observed along other passive margins worldwide, this process is inferred to be a large-scale slope instability.
- Seafloor fault scarps suggest active deformation in the area even if further investigations are needed to better understand the deformation context (i.e., tectonic, gravitative or both) and the related seismotectonic implications.
- Derived fault dimensions (e.g., for F3) and recurrence time interval are compatible with the magnitudes and return period estimated for large historical earthquakes in the area (e.g., the 1693 and 1169 events) although other seismic sources such as the 80 km-long North Alfeo Fault (Gutscher

et al., 2016 and **Figure 9** for location) must be considered as well in the seismotectonic framework of the Western Ionian Basin (see Gutscher et al., 2006).

Finally, our data provide additional information to consider reactivation of the Malta Escarpment as one of the potentially causative processes from which destructive seismic events in the area nucleated (see also Bianca et al., 1999; Azzaro and Barbano, 2000; Argnani and Bonazzi, 2005; Argnani et al., 2012). Assuming a prevailing tectonic component of deformation during the Quaternary, our data could provide useful information to improve databases concerning potential seismogenic sources in Italy (e.g., DISS or ITHACA) and contribute to a better assessment of the seismic hazard in the densely populated SE Sicily.

DATA AVAILABILITY STATEMENT

The original contributions presented in the study are included in the article/**Supplementary Material**, further inquiries can be directed to the corresponding author.

AUTHOR CONTRIBUTIONS

GB: work planning, conceptualization, seismic data interpretation, data analysis and interpretation of results, review of the literature data, geodynamics consideration, figures preparation, writing the final version of the manuscript, supervision, funding acquisition. SG: seismic data interpretation, field data measurement/elaboration, 3D modeling, stress-field and slip tendency computation, writing initial draft of the manuscript, draft figures preparation. FG and SK: POS496 seismic data acquisition and processing, critical reading of the manuscript. M-AG: planned the CIRCEE marine geophysical survey, seismic data acquisition, critical reading of the manuscript. CM: geodynamic considerations, review of the literature data, critical reading of the manuscript, funding acquisition, supervision.

SUPPLEMENTARY MATERIAL

The Supplementary Material for this article can be found online at: https://www.frontiersin.org/articles/10.3389/feart.2020.594176/full#supplementary-material.

REFERENCES

Adam, J., Reuther, C.-D., Grasso, M., and Torelli, L. (2000). Active fault kinematics and crustal stresses along the Ionian margin of southeastern Sicily. *Tectonophysics* 326, 217–239. doi:10.1016/S0040-1951(00)00141-4

Allmendinger, R. W., Cardozo, N., and Fisher, D. (2012). *Structural geology algorithms: vectors and tensors in structural geology* Cambridge, England: Cambridge University Press.

Amato, A., Azzara, R., Basili, A., Chiaraba, C., Cocco, M., Di Bona, M., et al. (1995). Main shock and aftershocks of the December 13, 1990 Eastern Sicily earthquake. *Ann. Geophys.* 38 (2), 255–266. doi:10.4401/ag-4122

Argnani, A., Armigliato, A., Pagnoni, G., Zaniboni, F., Tinti, S., and Bonazzi, C. (2012). Active tectonics along the submarine slope of south-eastern sicily and the source of the 11 january 1693 earthquake and tsunami. *Nat. Hazards Earth Syst. Sci.* 12 (5), 1311–1319. doi:10.5194/nhess-12-1311-2012

Argnani, A., and Bonazzi, C. (2005). Malta Escarpment fault zone offshore eastern Sicily: Pliocene-Quaternary tectonic evolution based on new multichannel seismic data. *Tectonics* 24, TC4009. doi:10.1029/2004TC001656

Argnani, A., and Bonazzi, C. (2002). Tectonics of eastern Sicily offshore: preliminary results from the MESC 2001 marine seismic cruise. *Boll. Geofis. Teor. Appl.* 43 (3–4), 177–193.

Argnani, A., Mazzarini, F., Bonazzi, C., Bisson, M., and Isola, I. (2013). The deformation offshore of Mount Etna as imaged by multichannel seismic reflection profiles. *J. Volcanol. Geotherm. Res.* 251, 50–64. doi:10.1016/j.jvolgeores.2012.04.016

A. Rovida, M. Locati, R. Camassi, B. Lolli, and P. Gasperini (2016). *CPTI15, the 2015 version of the parametric catalogue of Italian earthquakes* Rome, Italy: Istituto Nazionale di Geofisica e Vulcanologia.

Azzaro, R., and Barbano, M. S. (2000). Analysis of the seismicity of southeastern Sicily: a proposed tectonic interpretation. *Ann. Geofisc.* 43 (1), 171–188. doi:10.4401/ag-3628

Bai, T., Maerten, L., Gross, M. R., and Aydin, A. (2002). Orthogonal cross joints: do they imply a regional stress rotation? *J. Struct. Geol.* 24, 77–88. doi:10.1016/S0191-8141(01)00050-5

Bai, T., and Pollard, D. D. (2000). Fracture spacing in layered rocks: a new explanation based on the stress transition. *J. Struct. Geol.* 22, 43–57. doi:10.1016/S0191-8141(99)00137-6

Barbano, M. S., Rigano, R., Cosentino, M., and Lombardo, G. (2001). Seismic history and hazard in some localities of south-eastern Sicily. *Boll. Geofis. Teor. Appl.* 42 (1–2), 107–120.

Barbano, M. S., and Rigano, R. (2001). Earthquake sources and seismic hazard in south-eastern Sicily. *Ann. Geophys.* 44, 723–738. doi:10.4401/ag-3570

Barbano, M. S. (1985). "The val di Noto earthquake of january 11, 1693," in *Atlas of isoseismal maps of Italian earthquakes, CNR-PFG, quad* Bologna: Consiglio nazionale delle ricerche, Vol. 2A, 48–49.

Barreca, G. (2014). Geological and geophysical evidences for mud diapirism in south-eastern Sicily (Italy) and geodynamic implications. *J. Geodyn.* 82, 168–177. doi:10.1016/j.jog.2014.02.003

Barreca, G., Scarfì, L., Cannavò, F., Koulakov, I., and Monaco, C. (2016). New structural and seismological evidence and interpretation of a lithospheric-scale shear zone at the southern edge of the Ionian subduction system (centraleastern Sicily, Italy). *Tectonics* 35, 1489–1505. doi:10.1002/2015tc004057

Ben-Avraham, Z., and Grasso, M. (1991). Crustal structure variations and transcurrent faulting at the eastern and western margins of the eastern Mediterranean. *Tectonophysics* 75, 269–277. doi:10.1016/0040-1951(91)90326-N

Bianca, M., Monaco, C., Tortorici, L., and Cernobori, L. (1999). Quaternary normal faulting in southeastern Sicily (Italy): a seismic source for the 1693 large earthquake. *Geophys. J. Int.* 139, 370–394. doi:10.1046/j.1365-246x.1999.00942.x

Bianchi, F., Carbone, S., Grasso, M., Invernizzi, G., Lentini, F., LongarettiMerlini, G. S., et al. (1987). Sicilia orientale: profilo geologico Nebrodi-Iblei. *Mem. Soc. Geol. It.* 38, 429–458.

Billi, A., Minelli, L., Orecchio, B., and Presti, D. (2010). Constraints to the cause of three historical tsunamis (1908, 1783, and 1693) in the messina straits region, Sicily, Southern Italy. *Seismol Res. Lett.* 81 (6), 907–915. doi:10.1785/gssrl.81.6.907

Billi, A., Porreca, M., Faccenna, C., and Mattei, M. (2006). Magnetic and structural constraints for the noncylindrical evolution of a continental forebulge (Hyblea, Italy). *Tectonics* 25, TC3011. doi:10.1029/2005TC001800

Bingham, C. (1974). An antipodally symmetric distribution on the sphere. *Ann. Stat.* 2 (6), 1201–1225.

Bott, M. H. P. (1959). The mechanics of oblique slip faulting. *Geol. Mag.* 96, 109–117.

Burollet, P. F., Mugniot, G. M., and Sweeney, P. (1978). "The geology of the pelagian block: the margins and basins of southern Tunisia and tripolitania," in *The Ocean basins and margins 4 B* Editors Nairn, A. E. M., and Stehli, F. G. (New York, NY: Plenum Press), 331–339.

Boschi, E., Ferrari, G., Gasperini, P., Guidoboni, E., Smriglio, G., and Valensise, G. (1995). Catalogo dei Forti Terremoti in Italia dal 461 a.c, al 1980. Roma, Italy: Istituto Nazionale di Geofisica, S.G.A.

Butler, R. W. H., Maniscalco, R., Sturiale, G., and Grasso, M. (2015). Stratigraphic variations control deformation patterns in evaporite basins: Messinian examples, onshore and offshore Sicily (Italy). *J. Geol. Soc.* 172, 113–124. doi:10.1144/jgs2014-024

Camerlenghi, A., Del Ben, A., Hubscher, C., Forlin, E., Geletti, R., Brancatelli, G., et al. (2019). Seismic markers of the Messinian salinity crisis in the deep Ionian Basin. *Basin Res.* 32, 716–738. doi:10.1111/bre.12392

Carbone, S., Grasso, M., and Lentini, F. (1986). *Carta geologica del settore nord-orientale ibleo (Sicilia S.E.), scala 1:50.000* Firenze: SELCA.

Carbone, S., Grasso, M., and Lentini, F. (1984). *Carta geologica della Sicilia sud-orientale, scala 1:100.000* Firenze: SELCA.

Cardozo, N., and Allmendinger, R. W. (2013). Spherical projections with OSXStereonet. *Comput. Geosci.* 51, 193–205. doi:10.1016/j.cageo.2012.07.021

Cartwright, J. A., Trudgill, B. D., and Mansfield, C. S. (1995). Fault growth by segment linkage: an explanation for scatter in maximum displacement and trace length data from the Canyonlands Grabens of SE Utah. *J. Struct. Geol.* 17 (9), 1319–1326. doi:10.1016/0191-8141(95)00033-A

Casero, P., Cita, M. B., Croce, M., and De Micheli, A. (1984). Tentativo di interpretazione evolutiva della Scarpata di Malta basata sui dati geologici e geofisici. *Mem. Soc. Geol. It.* 27, 233–254.

Catalano, R., Doglioni, C., and Merlini, S. (2001). On the mesozoic ionian basin. *Geophys. J. Int.* 144, 49–64. doi:10.1046/j.0956-540X.2000.01287.x

Cifelli, F., Rossetti, F., Mattei, M., Hirt, A. M., Funiciello, R., and Tortorici, L. (2004). An AMS, structural and paleomagnetic study of quaternary deformation in eastern Sicily. *J. Struct. Geol.* 26, 29–46. doi:10.1016/S0191-8141(03)00092-0

Cogan, J., Rigo, L., Grasso, M., and Lerche, I. (1989). Flexural tectonics of southeastern sicily. *J. Geodyn.* 11 (3), 189–241. doi:10.1016/0264-3707(89)90007-0

Cultrera, F., Barreca, G., Scarfì, L., and Monaco, C. (2015). Fault reactivation by stress pattern reorganization in the Hyblean foreland domain of SE Sicily (Italy) and seismotectonic implications. *Tectonophysics* 661, 215–228. doi:10.1016/j.tecto.2015.08.043

De Guidi, G., Caputo, R., and Scudero, S. (2013). Regional and local stress field orientation inferred from quantitative analyses of extension joints: case study from southern Italy. *Tectonics* 32, 1–13. doi:10.1002/tect.20017

Dellong, D., Klingelhoefer, F., Kopp, H., Graindorge, D., Margheriti, L., Moretti, M., et al. (2018). Crustal structure of the Ionian basin and eastern Sicily margin: results from a wide-angle seismic survey. *J. Geophys. Res. Solid Earth* 123, 2090–2114. doi:10.1002/2017JB015312

DISS Working Group (2018). Database of Individual Seismogenic Sources (DISS), Version 3.2.1: a compilation of potential sources for earthquakes larger than M 5.5 in Italy and surrounding areas. Available at: http://diss.rm.ingv.it/diss/ (Accessed December 3, 2018).

Doglioni, C., Innocenti, F., and Mariotti, G. (2001). Why Mt Etna? *Terra. Nova* 13 (1), 25–31. doi:10.1046/j.1365-3121.2001.00301.x

D'Agostino, N., and Selvaggi, G. (2004). Crustal motion along the eurasia-nubia plate boundary in the calabrian arc and sicily and active extension in the messina straits from GPS measurements. *J. Geophys. Res.* 109, B11402. doi:10.1029/2004JB002998

Fabbri, A., Rossi, S., Sartori, R., and Barone, A. (1982). Evoluzione neogenica dei margini marini dell'Arco Calabro-Peloritano: implicazioni geodinamiche. *Mem. Soc. Geol. It.* 24, 357–366.

Gallais, F., Gutscher, M.-A., Graindorge, D., Chamot-Rooke, N., and Klaeschen, D. (2011). A Miocene tectonic inversion in the Ionian Sea (central Mediterranean): evidence from multichannel seismic data. *J. Geophys. Res.* 116, B12108. doi:10.1029/2011JB008505

Ghisetti, F., and Vezzani, L. (1980). The structural features of the Hyblean Plateau and the Mount Judica area (south-eastern Sicily): a microtectonic contribution to the deformational history of the Calabrian arc. *Boll. Soc. Geol. Ital.* 99, 55–102.

Govers, R., and Wortel, M. J. R. (2005). Lithosphere tearing at STEP faults: response to edges of subduction zones. *Earth Planet Sci. Lett.* 236 (1–2), 505–523. doi:10.1016/j.epsl.2005.03.022

Grasso, M., Lentini, F., Nairn, A. E. M., and Vigliotti, M. (1983). A geological and paleomagnetic study of the Hyblean volcanic rocks. *Tectonophysics* 98 (3-4), 271–295. doi:10.1016/0040-1951(83)90298-6

Grasso, M., and Lentini, F. (1982). Sedimentary and tectonic evolution of the eastern Hyblean Plateau (South-eastern Sicily) during late cretaceous to quaternary time. *Palaeogeogr. Palaeoclimatol. Palaeoecol.* 39, 261–280. doi:10.1016/0031-0182(82)90025-6

Grasso, M., Pedley, H. M., Behncke, B., Maniscalco, R., and Sturiale, G. (2004). "Integrated the neogene-frontiers quaternary sedimentation and volcanism in the northern Hyblean Plateau (sicily)," in *Mapping geology in Italy* Editors G. Pasquarè and C. Venturini (Roma, IT: APAT), 159–166.

Grasso, M., and Reuther, C. D. (1988). The western margin of the Hyblean Plateau: a neotectonic transform system on the SE Sicilian foreland. *Ann. Tect.* 2, 107–120.

Grenerczy, G., Sella, G., Stein, S., and Kenyeres, A. (2005). Tectonic implications of the GPS velocity field in the northern Adriatic region. *Geophys. Res. Lett.* 32, L16311. doi:10.1029/2005GL022947

Gross, F., Krastel, S., Geersen, J., Hinrich, B. J., Ridente, D., Chiocci, F. L., et al. (2016). The limits of seaward spreading and slope instability at the continental margin offshore Mt. Etna, imaged by high-resolution 2D seismic data. *Tectonophysics* 667, 63–76. doi:10.10164/j.tecto.2015.11.011

Gutscher, M.-A., Dominguez, S., Mercier de Lepinay, B., Pinheiro, L., Gallais, F., Babonneau, N., et al. (2016). Tectonic expression of an active slab tear from high-resolution seismic and bathymetric data offshore Sicily (Ionian Sea). *Tectonics* 35, 39–54. doi:10.1002/2015TC003898

Gutscher, M.-A., Kopp, H., Krastel, S., Bohrmann, G., Garlan, T., Zaragosi, S., et al. (2017). Active tectonics of the Calabrian subduction revealed by new multi-beam bathymetric data and high-resolution seismic profiles in the Ionian Sea (Central Mediterranean). *Earth Planet Sci. Lett.* 461, 61–72. doi:10.1016/j.epsl.2016.12.020

Gutscher, M.-A., Roger, J., Baptista, M. A., Miranda, J. M., and Tinti, S. (2006). The source of the 1693 Catania earthquake and tsunami (Southern Italy): new evidence from tsunami modeling of a locked subduction fault plane. *Geophys. Res. Lett.* 33, L08309. doi:10.1029/2005GL025442

Henriquet, M., Dominguez, S., Barreca, G., Malavieille, J., Cadio, C., and Monaco, C. (2019). Deep origin of the dome-shaped Hyblean Plateau, southeastern sicily: a new tectono-magmatic model. *Tectonics* 38 (12), 4488–4515. doi:10.1029/2019TC005548

Hsü, K. J., Montadert, L., Bernoulli, D., Bizon, G., Cita, M., Erickson, A., et al. (1978). "Site 374: messina abyssal plain part 1," in *Initial reports of the deep-sea drilling project* Washington, DC: U.S. Government Printing Office, Vol. 42.

Jenny, S., Goes, S., Giardini, D., and Kahle, H.-G. (2006). Seismic potential of southern Italy. *Tectonophysics* 415, 81–101. doi:10.1016/j.tecto.2005.12.003

Kokinou, E., Vafidis, A., Loucogiannakis, M., and Louis, I. (2013). Deep seismic imaging and velocity estimation in Ionian Sea. *J. Balkan Geophys. Soc.* 6 (2), 100–116.

Krastel, S. (2016). "Short cruise report: MAGOMET—offshore flank movement of mount Etna and associated landslide hazard in the Ionian Sea (mediterranean sea)," in RV POSEIDON-CRUISE POS496, Malaga, Catania, March 24–April 4, 2016 (Christian-Albrechts-Universität zu Kiel, Institute of Geosciences), 8.

Le Meur, D. (1997). *Etude géophysique de la structure profonde et de la tectonique active de la partie occidentale de la Ride Méditerranéenne* [Ph.D. thesis]. Paris (FR): University of Paris XI.

Leonard, M. (2010). Earthquake fault scaling: self-consistent relating of rupture length, width, average displacement, and moment release. *Bull. Seismol. Soc. Am.* 100 (5A), 1971–1988. doi:10.1785/0120090189

Lofi, J., Deverchère, J., Gaullier, V., Gillet, H., Gorini, C., Guennoc, P., et al. (2011). Seismic atlas of the messinian salinity crisis markers in the mediterranean and black seas. *Mém. Soc. Géol. CCGM* 179, 1–72.

Maesano, F. E., Tiberti, M. M., and Basili, R. (2020). Deformation and fault propagation at the lateral termination of a subduction zone: the alfeo Fault system in the calabrian arc, southern Italy. *Front. Earth Sci.* 8, 107. doi:10.3389/feart.2020.00107

Maesano, F. E., Tiberti, M. M., and Basili, R. (2017). The Calabrian Arc: three-dimensional modelling of the subduction interface. *Sci. Rep.* 7, 8887. doi:10.1038/s41598-017-09074-8

Mastrolembo, V. B., Serpelloni, E., Argnani, A., Bonforte, A., Bürgmann, R., Anzidei, M. P., et al. (2014). Fast geodetic strain-rates in eastern sicily (southern Italy): new insights into block tectonics and seismic potential in the area of the great 1693 earthquake. *Earth Planet Sci. Lett.* 404, 77–88. doi:10.1016/j.epsl.2014.07.025

Matos, R. M. D. (2000). "Tectonic evolution of the equatorial south atlantic," in *The Brazilian and west African equatorial margins comprise America in, Atlantic rifts and continental margins* Editors W. Mohriak and M. Taiwani (Hoboken, NJ: Wiley), 115, 331–354.

Mattia, M., Bruno, V., Cannavò, F., and Palano, M. (2012). Evidences of a contractional pattern along the northern rim of the Hyblean Plateau (sicily, Italy) from GPS data. *Geol. Acta* 10 (1), 63–70. doi:10.1344/105.000001705

Micallef, A., Camerlenghi, A., Garcia-Castellanos, D., Cunarro Otero, D., Gutscher, M.-A., Barreca, G., et al. (2018). Evidence of the zanclean megaflood in the eastern Mediterranean basin. *Sci. Rep.* 8 (1), 1078. doi:10.1038/s41598-018-19446-3

Micallef, A., Camerlenghi, A., Georgiopoulou, A., Garcia-Castellanos, D., Gutscher, M.-A., Lo Iacono, C., et al. (2019). Geomorphic evolution of the Malta Escarpment and implications for the Messinian evaporative drawdown in the eastern Mediterranean Sea. *Geomorphology* 327, 264–283. doi:10.1016/j.geomorph.2018.11.012

Monaco, C., and Tortorici, L. (2000). Active faulting in the Calabrian arc and eastern Sicily. *J. Geodyn.* 29 (3–5), 407–424. doi:10.1016/S0264-3707(99)00052-6

Montone, P., Mariucci, M. T., and Pierdominici, S. (2012). The Italian present-day stress map. *Geophys. J. Int.* 189 (2), 705–716. doi:10.1111/j.1365-246X.2012.05391.x

Morris, A., Ferrill, D. A., and Henderson, D. B. (1996). Slip-tendency analysis and fault reactivation. *Geology* 24, 275–278. doi:10.1130/0091-7613(1996)024<0275:STAAFR>2.3.CO;2

Mulargia, F., Broccio, F., Achilli, V., and Baldi, P. (1985). Evaluation of a seismic quiescence pattern in southeastern Sicily. *Tectonophysics* 116, 335–364. doi:10.1016/0040-1951(85)90214-8

Musumeci, C., Scarfì, L., Palano, M., and Patanè, D. (2014). Foreland segmentation along an active convergent margin: new constraints in southeastern Sicily (Italy) from seismic and geodetic observations. *Tectonophysics* 630, 137–149. doi:10.1016/j.tecto.2014.05.017

Palano, M., Ferranti, L., Monaco, C., Mattia, M., Aloisi, M., Bruno, V., et al. (2012). GPS velocity and strain fields in Sicily and southern Calabria, Italy: updated geodetic constraints on tectonic block interaction in the central Mediterranean. *J. Geophys. Res.* 117, B07401. doi:10.1029/2012JB009254

Patacca, E., Scandone, P., Giunta, G., and Liguori, V. (1979). Mesozoic paleotectonic evolution of the Ragusa zone (southern Sicily). *Geol. Rom.* 18, 331–369.

Pedley, M., and Grasso, M. (1992). Miocene syntectonic sedimentation along the western margins of the Hyblean-Malta platform: a guide to plate margin processes in the central Mediterranean. *J. Geodyn.* 15 (1–2), 19–37. doi:10.1016/0264-3707(92)90004-C

Piatanesi, A., and Tinti, S. (1998). A revision of the 1693 eastern Sicily earthquake and tsunami. *J. Geophys. Res. Solid Earth* 103 (B2), 2749–2758. doi:10.1029/97JB03403

Polonia, A., Torelli, L., Artoni, A., Carlini, M., Faccenna, C., Ferranti, L., et al. (2016). The Ionian and Alfeo-Etna fault zones: new segments of an evolving plate boundary in the central Mediterranean Sea? *Tectonophysics* 675, 69–90. doi:10.1016/j.tecto.2016.03.016

Polonia, A., Torelli, L., Gasperini, L., Cocchi, L., Muccini, F., Bonatti, E., et al. (2017). Lower plate serpentinite diapirism in the Calabrian Arc subduction complex. *Nat. Commun.* 8, 2172. doi:10.1038/s41467-017-02273-x

Polonia, A., Torelli, L., Gasperini, L., and Mussoni, P. (2012). Active faults and historical earthquakes in the messina straits area (Ionian Sea). *Nat. Hazards Earth Syst. Sci.* 12, 2311–2328. doi:10.5194/nhess-12-2311-2012

Pondrelli, S.[Dataset] (2002). European-mediterranean regional centroid-moment tensors catalog (RCMT). (INGV) Istituto Nazionale di Geofisica e Vulcanologia. Available at: https://doi.org/10.13127/rcmt/euromed (Accessed 2002).

Presti, D., Billi, A., Orecchio, B., Totaro, C., Faccenna, C., and Neri, G. (2013). Earthquake focal mechanisms, seismogenic stress, and seismotectonics of the Calabrian Arc, Italy. *Tectonophysics* 602 153–175. doi:10.1016/j.tecto.2013.01.030

Ragg, S., Grasso, M., and Müller, B. (1999). Patterns of tectonic stress in Sicily from borehole breakout observations and finite element modeling. *Tectonics* 18 (4), 669–685. doi:10.1029/1999TC900010

Scandone, P., Patacca, E., Radoicic, R., Ryan, W. B. F., Cita, M. B., Rawson, M., et al. (1981). Mesozoic and cenozoic rocks from Malta escarpment (Central Mediterranean). *AAPG Bull.* 65 (7), 1299–1319. doi:10.1306/03B5949F-16D1-11D7-8645000102C1865D

Scarfì, L., Barberi, G., Musumeci, C., and Patanè, D. (2016). Seismotectonics of northeastern Sicily and Southern Calabria (Italy): new constraints on the tectonic structures featuring in a crucial sector for the Central Mediterranean geodynamics. *Tectonics* 35, 812–832. doi:10.1002/2015TC00402

Scarfì, L., Messina, A., and Cassisi, C. (2013). Sicily and Southern Calabria focal mechanism database: a valuable tool for the local and regional stress field determination. *Ann. Geophys.* 56, 6109. doi:10.4401/ag-6109

Şengör, A. M. C. (1979). Mid-mesozoic closure of permo-triassic tethys and its implications. *Nature* 279, 590–593. doi:10.1038/279590a0

Servizio Geologico d'Italia (2011). Foglio 641 Augusta della Carta Geologica d'Italia alla scala 1:50.000. Coordinatore scientifico Carbone S. Direttore dei rilevamenti Lentini F. Note illustrative a cura di Carbone S. (ISPRA). 247.

Sirovich, L., and Pettenati, F. (2001). Test of source-parameter inversion of the intensities of a 54,000-death shock of the seventeenth century in southeastern Sicily. *Bull. Seismol. Soc. Am.* 91, 792–811.

Tinti, S., Armigliato, A., and Bortolucci, E. (2001). Contribution of tsunami data analysis to constrain the seismic source: the case of the 1693 eastern Sicily earthquake. *J. Seismol.* 5 (1), 41–61. doi:10.1023/A:1009817601760

Tinti, S., Maramai, A., and Graziani, L. (2004). The new catalogue of Italian tsunamis. *Nat. Hazards* 33, 439–465. doi:10.1023/B:NHAZ.0000048469.51059.65

Trippetta, F., Petricca, P., Billi, A., Collettini, C., Cuffaro, M., Lombardi, A. M., et al. (2019). From mapped faults to fault-length earthquake magnitude (FLEM): a test on Italy with methodological implications. *Solid Earth* 10, 1555–1579. doi:10.5194/se-10-1555-2019

Wallace, R. E. (1951). Geometry of shearing stress and relation to faulting. *J. Geol.* 59, 118–130. doi:10.1086/625831

Ward, S. (1994). Constraints on the seismotectonics of the central mediterranean from very long baseline interferometry. *Geophys. J. Int.* 117, 441–452. doi:10.1111/j.1365-246X.1994.tb03943.x

Wells, D. L., and Coppersmith, K. J. (1994). New empirical relationships among magnitude, rupture length, rupture width, rupture area, and surface displacement. *Bull. Seismol. Soc. Am.* 84 (4), 974–1002.